

INFORMATION TO USERS

This manuscript has been reproduced from the microfilm master. UMI films the text directly from the original or copy submitted. Thus, some thesis and dissertation copies are in typewriter face, while others may be from any type of computer printer.

The quality of this reproduction is dependent upon the quality of the copy submitted. Broken or indistinct print, colored or poor quality illustrations and photographs, print bleedthrough, substandard margins, and improper alignment can adversely affect reproduction.

In the unlikely event that the author did not send UMI a complete manuscript and there are missing pages, these will be noted. Also, if unauthorized copyright material had to be removed, a note will indicate the deletion.

Oversize materials (e.g., maps, drawings, charts) are reproduced by sectioning the original, beginning at the upper left-hand corner and continuing from left to right in equal sections with small overlaps.

ProQuest Information and Learning
300 North Zeeb Road, Ann Arbor, MI 48106-1346 USA
800-521-0600

UMI[®]

University of Alberta

Long-term Relationships Between Drought and Smoke-haze in Indonesia

by

Robert Dode Field



A thesis submitted to the Faculty of Graduate Studies and Research in partial fulfillment of the

requirements for the degree of Master of Science

in

Statistics

Department of Mathematical and Statistical Sciences

Edmonton, Alberta

Fall 2005



Library and
Archives Canada

Bibliothèque et
Archives Canada

0-494-09161-4

Published Heritage
Branch

Direction du
Patrimoine de l'édition

395 Wellington Street
Ottawa ON K1A 0N4
Canada

395, rue Wellington
Ottawa ON K1A 0N4
Canada

Your file *Votre référence*

ISBN:

Our file *Notre référence*

ISBN:

NOTICE:

The author has granted a non-exclusive license allowing Library and Archives Canada to reproduce, publish, archive, preserve, conserve, communicate to the public by telecommunication or on the Internet, loan, distribute and sell theses worldwide, for commercial or non-commercial purposes, in microform, paper, electronic and/or any other formats.

The author retains copyright ownership and moral rights in this thesis. Neither the thesis nor substantial extracts from it may be printed or otherwise reproduced without the author's permission.

AVIS:

L'auteur a accordé une licence non exclusive permettant à la Bibliothèque et Archives Canada de reproduire, publier, archiver, sauvegarder, conserver, transmettre au public par télécommunication ou par l'Internet, prêter, distribuer et vendre des thèses partout dans le monde, à des fins commerciales ou autres, sur support microforme, papier, électronique et/ou autres formats.

L'auteur conserve la propriété du droit d'auteur et des droits moraux qui protègent cette thèse. Ni la thèse ni des extraits substantiels de celle-ci ne doivent être imprimés ou autrement reproduits sans son autorisation.

In compliance with the Canadian Privacy Act some supporting forms may have been removed from this thesis.

Conformément à la loi canadienne sur la protection de la vie privée, quelques formulaires secondaires ont été enlevés de cette thèse.

While these forms may be included in the document page count, their removal does not represent any loss of content from the thesis.

Bien que ces formulaires aient inclus dans la pagination, il n'y aura aucun contenu manquant.


Canada

Abstract

Long-term analyses of Indonesia's serious smoke haze problem have been limited due to the lack of fire records or air quality measurements. In response, a monthly indicator of smoke haze has been developed for Indonesia using visibility observations. Visibility signals were developed for the fire prone regions of southern Sumatra and southern Kalimantan, and compared to several moisture indices to determine the relationship between drought and smoke haze from 1979 to 2003. Analysis of haze signals showed that (i) 1997 fire event was of an unprecedented magnitude, (ii) the 2002 haze event occurred under only moderate drought, and (iii) Indonesia's fire environment is becoming more sensitive. Nonlinear regression techniques showed that simple rainfall-based indices are preferable to complicated soil moisture models in predicting severe haze events, which have occurred historically when the 3-month total rainfall drops below 337.26mm (247.83, 404.93) in Sumatra and 414.25 mm (381.01, 467.89) in Kalimantan.

Acknowledgements

The support of numerous people is acknowledged. This work was initiated while at the Canadian Forest Service, working under the Southeast Asia Fire Danger Rating System Project. There, the initial encouragement of Bryan Lee and Bill de Groot in pursuing this research is gratefully appreciated, as is the guidance of Michael Brady during time spent in Indonesia. Tom Karl and Sam McGown at the National Oceanic and Atmospheric Administration (NOAA) National Climatic Data Center generously provided the bulk of the meteorological data for the analysis, and Mingyue Chen and Yun Fan at the NOAA Climate Prediction Centre provided technical support in using several of the moisture datasets. Orbita Roswintiarti at the Indonesian National Institute of Aeronautics and Space and Maznorizan Mohammad at the Malaysian Meteorological Service kindly provided several figures, and valuable information on Indonesia's meteorological network was given by Guswanto at the Indonesian Bureau of Meteorology and Geophysics. At the University of Alberta, Vic Adamowicz in the Department of Rural Economy and Peter Hooper in the Department of Mathematical and Statistical Sciences gave important advice on statistical methods, and Laura McIntyre provided much of the processed data.

I am especially grateful to my supervisor Sam Shen, for his unwavering support over the course of my program, and of course to my wife Norah for her patience.

This work was funded in part by the Canadian International Development Agency and the Southeast Asia Regional Committee for START.

Table of contents

1. Introduction.....	1
1.1. Context.....	1
1.2. Characterizations of the 1997/98 haze disaster.....	1
1.3. Long term characterization studies	3
1.4. Impacts of fire and smoke in Indonesia	5
1.5. Causes of fire and smoke in Indonesia	6
1.6. Historical haze indicator	8
1.7. Study objectives	9
2. Data.....	11
2.1. Visibility data.....	11
2.2. Moisture indices.....	16
2.3. Land cover for peat identification.....	21
2.4. Wind streamlines from Reanalysis data.....	21
3. Methods.....	23
3.1. Visibility dataset development.....	23
3.2. Drought and haze analysis	24
4. Results and Discussion	37
4.1. Meta-data characteristics	37
4.2. Qualitative analysis of haze and moisture signals	39
4.3. Regression results	47
4.4. Moisture thresholds.....	56
5. Conclusions.....	65
5.1. Key results	65
5.2. Suggestions for further work	67
References.....	70
Appendix A: Model parameter estimates and residuals	80

List of tables

Table 1. Selected analysis stations for Sumatra and Kalimantan	27
Table 2. Timing and severity of major haze events in Sumatra and Kalimantan.	43
Table 3. Adjusted coefficient of determination (R^2) for different predictors and regression models, for different intervals of the moisture indicators	54
Table 4. Summary of moisture threshold estimates.....	61
Table 5. 3-month rainfall interpretive guidelines for Sumatra and Kalimantan based on PRECL rainfall.....	64
Table 6. Bootstrapped parameter estimates for change point models.	80
Table 7. Bootstrapped parameter estimates for sigmoidal models.....	81
Table 8. Parameter estimates for ALB model.....	82

List of figures

Figure 1. Monthly rainfall in Palembang, South Sumatra and Victoria, British Columbia.....	7
Figure 2. Medium-range visibility observation contours for Kuala Lumpur, Malaysia	12
Figure 3. Weather station distribution over Indonesia.....	15
Figure 4. Average wind streamlines during July and September	27
Figure 5. Visibility stations selected for analysis in Sumatra and Kalimantan	28
Figure 6. Example sigmoidal curve with first and second derivatives.	32
Figure 7. Total number of observations per year across all Indonesian stations	37
Figure 8. Monthly observation totals for Sumatra and Kalimantan.....	38
Figure 9. Extinction coefficient and moisture signals for Sumatra..	41
Figure 10. Extinction coefficient and moisture signals for Kalimantan..	42
Figure 11. GPCP rainfall and extinction coefficient for severe haze events, Sumatra	46
Figure 12. GPCP rainfall and extinction coefficient for severe haze events, Kalimantan.....	47
Figure 13. Fitted regression models for Sumatra.....	52
Figure 14. Fitted regression models for Kalimantan	53
Figure 15. 850 mb monthly mean winds from the NCAR Reanalysis	55
Figure 16. 850 mb monthly mean winds from the NCAR Reanalysis	56
Figure 17. Interval-based thresholds for Sumatra.....	59
Figure 18. Interval-based thresholds for Kalimantan.	60
Figure 19. Threshold estimates for different moisture indices and models.....	62
Figure 20. Residuals from fitted models for Sumatra.....	83
Figure 21. Residuals from fitted models for Kalimantan.	84

List of abbreviations

ADB	Asian Development Bank
ALB	Adaptive Logistic Basis regression
ATSR	Along Track Scanning Radiometer
AVHRR	Advanced Very High Resolution Radiometer
B_{ext}	Extinction coefficient
CAMS	Climate Anomaly Monitoring System
DC	Drought Code component of the Canadian Forest Fire Weather Index System
ENSO	El Niño Southern Oscillation
ERS-2 SAR	European Radar Satellite-2-Synthetic Aperture Radar
GHCN	Global Historical Climate Network
GPCC	Global Precipitation Climatology Centre
GPCP	Global Precipitation Climatology Project rainfall dataset
GSOD	Global Summary of the Day dataset at NCDC
GTS	Global Telecommunications System
ISH	Integrated Surface Hourly dataset at NCDC
LCL	Lower confidence level
NASA	National Aeronautics and Space Administration
NCAR	National Centre for Atmospheric Research
NCDC	National Climatic Data Center
NCEP	National Centre for Environmental Prediction
NOAA	National Oceanic and Atmospheric Administration
PDSI	Palmer Drought Severity Index
PRECL	Precipitation over Land dataset from NCEP
SOILM	Soil moisture dataset from NCEP
TOMS AI	Total Ozone Mapping Spectrometer Aerosol Index
UCL	Upper confidence level

WMO World Meteorological Organization
WWF World Wide Fund for Nature

1. Introduction

1.1. Context

Biomass burning represents a significant contribution to global emissions of greenhouse gases (GHGs) and aerosols [Enhalt et al., 2001]. A recent study by Langenfelds et al. [2002] showed that the interannual growth of CO₂ and other GHG's is not steady, but occurs irregularly over timescales of 2-5 years, and that this pattern of growth could not be explained by fossil fuel burning. They proposed biomass burning as a plausible source of this interannual growth, showing that sharp increases of GHG's in 1994/1995 and 1997/1998 could be attributed to anomalously high emissions from biomass burning. Zeng et al. [2005] estimated that biomass burning represents roughly 20% of this mean inter-annual carbon flux anomaly, mainly with an increase in tropical fire in response to drought conditions. During El Niño-induced droughts, Southeast Asia becomes the main source of C-emissions from biomass burning, representing 60% of the total global emissions from biomass burning [Van der Werf et al., 2004]. Knorr et al. [2005] recently suggested Indonesian biomass burning as the cause of the large 1997/1998 increase in atmospheric CO₂ at Mauna Loa, Hawaii, the principal monitoring location of global atmospheric CO₂ concentration.

All accounts indicate that tropical biomass burning emissions are increasing, and will continue to do so owing to increasing economic development [Brasseur et al., 1998; Nichol, 1998; Hendon 2003] and possible positive feedbacks between deforestation and fires in tropical areas [Siegert et al., 2001; Cochrane, 2003]. In these studies, biomass burning in Indonesia is recognized as a singularly large tropical emission source. The remainder of this chapter reviews the 1997/98 fire and haze disaster in Indonesia, longer term characterization studies, the causes and impacts of the fire, and the rationale for this study.

1.2. Characterizations of the 1997/98 haze disaster

Owing to its severity, the 1997/98 fire and haze episode in Indonesia attracted significant investigation. The event lasted from June to November 1997 in the southern provinces of Sumatra and Kalimantan, and was followed by a smaller event

during a localized drought in East Kalimantan province from February to May of 1998 [Siegert and Hoffman, 2000]. To characterize the extent of fire locations during the event, remote sensing has been used exclusively because of the absence of ground-truthed fire records collected consistently across regions and jurisdictions [Page et al., 2002]. Fang and Huang [1998] detected fires in Sumatra and Kalimantan during September 1997 using Advanced Very High Resolution Radiometer (AVHRR) satellite data, showing the majority of fire activity to be in the coastal areas of southeastern Sumatra and southern Kalimantan. An AVHRR dataset was also used to investigate the underlying land-use and biophysical factors promoting fire occurrence during 1997, particularly land management classification [Stolle and Lambin, 2003]. The Along Track Scanning Radiometer (ATSR) sensor provides similar spatial resolution to the AVHRR hotspots, and was used to also show Sumatra and Kalimantan as the main fire prone regions of Indonesia by Heil and Goldammer [2001]. Siegert and Hoffman [2000] combined AVHRR data with high-resolution European Radar Satellite-2-Synthetic Aperture Radar (ERS-2 SAR) satellite imagery to estimate the total area burned in the province of East Kalimantan during 1998, a major fire-prone region on the island of Borneo. Liew et al. [1999] also performed a high-resolution mapping of the area burned in 1997 in southern Kalimantan, by comparing pre-fire to post-fire images.

To study smoke emissions from the 1997 fires, both remote sensing techniques and direct measurements have been used. The most commonly used remote sensing source is the National Aeronautics and Space Administration's (NASA) Total Ozone Mapping Spectrometer Aerosol Index Product (TOMS AI) [Hsu et al., 1996; Herman et al., 1997]. Originally deployed to detect global changes in stratospheric ozone, the TOMS AI is a derived product, calibrated to detect aerosols in the free troposphere. Smoke emissions from the 1997 Indonesian episode were detected in several TOMS-based analyses [Chandra et al., 1998; Nakajima et al., 1999; Gutman et al., 2000]. Burrows et al. [1999] also described the increase in detected ozone and trace gases seen over Borneo, as part of the Global Ozone Monitoring Experiment.

Direct measurements of atmospheric pollution were also taken during the 1997/98 episode, both at the surface and in the upper atmosphere, in Indonesia, and in

downwind receptor locations affected by transboundary haze transport. Surface-based characterizations of the smoke haze in 1997 were provided by Heil and Goldammer [2000] for Sumatra and Kalimantan, using several different indicators. Discontinuous observations of particulate matter with diameter less than 10 μm (PM_{10}) and total suspended particulate matter (TSP) were taken for two sites in each of Sumatra and Kalimantan, for limited periods during September to November 1997. In situ air quality measurements have been sparse, as Indonesia has not yet established a comprehensive long-term air quality network [Nichol, 1998; Radojevic, 2000].

Aircraft measurements in Tsutsumi et al. [1999] describe the regional extent of the 1997 haze, and observed significantly larger particle sizes in Indonesian emissions compared to emissions from fires in Australia. Sawa et al. [1999] also observed markedly different chemical composition from Indonesian fires than to the Australian fires, attributing differences primarily to the smoldering peat combustion seen in Indonesia, which was absent in Australia. Ikegami et al. [2001] further confirmed the significance of the extensive smoldering peat combustion in Indonesia, as reflected by the particulate matter composition of emissions over Kalimantan.

Yonemura et al. [2002b] showed ozone enhancements over Singapore during September to November 1997 and February to May 1998. In-situ measurements of air quality in Peninsular Malaysia by Fang et al. [1999], Von Hoyningen-Huene et al. [1999], and Khandekar et al. [2000] documented the transboundary effects from burning in Indonesia, although some smoke-haze is known to have originated from local sources in Malaysia. Enhanced ozone concentration was also detected directly as far northward as Hong Kong [Chan et al., 2001], and Indonesia was identified as the primary source through back trajectory simulations and analysis of the TOMS data.

1.3. Long term characterization studies

Several studies compared the relative magnitudes of haze events since 1980 from different perspectives. Nichol [1998] noted that though Indonesian droughts in 1994 and 1997/98 were less severe than during the 1982/83 El Niño, fire and consequent regional emissions were much more severe, owing to increasing rates of

transmigration and associated land conversion, as described in Fearnside [1997]. Nichol [1997] contended that smoke-haze in Indonesia will continue to worsen as transmigration and land conversion in Indonesia progress.

Radojevic [2003] provided a qualitative regional comparison of the 1994 and 1997 events, showing the increase in regional extent of haze from the 1994 event to the 1997/98 event. Bowen et al. [2001] also gave a largely qualitative, but descriptive review of the main haze episodes since 1980. Through their review of secondary sources, they estimated that 3 Mha of forest burned during the 1982/83 event, primarily on the island of Borneo, including Brunei and Malaysian Borneo. The 1987 event was less severe, with an estimate of 66 Kha burned, but which also included Sumatra. During 1991, 500 Kha was estimated to have burnt, with dense, but localized smoke-haze. Bowen et al. [2001] described the 1994 event as the first haze event of regional scope, with smoke-haze from Sumatra being transported to Peninsular Malaysia and smoke from Kalimantan transport to Malaysian Borneo, resulting from a total of 4.9 Mha burned. Although the 1997/98 event was thoroughly documented, area burned estimates varied greatly between institutions. Data summarized by the Asian Development Bank [ADB, 1999] yielded a total of 9.7 Mha burned across Sumatra and Kalimantan from May 1997 to March 1998. Bowen et al. [2001] and Nichol [1998] note that official area burned statistics were of dubious quality, given the political sensitivity of the fire and haze issue, and the resulting lack of standardization in gathering fire statistics.

Fujiwara et al. [1999] described the tropospheric ozone enhancements over a location in East Java during the fire events of 1994 and 1997 from burning in Kalimantan, as observed by ozonesonde measurements. Similarly, Yonemura et al. [2002a] detected upper-air ozone enhancements over Malaysia in 1994 and 1997, attributed to Indonesian biomass burning, during their study period from 1992 to 1999. Kita et al. [2000] and Thompson et al. [2001] provided the longest quantitative multi-year analysis, using TOMS AI data from 1979 to 2000. Confirming the description of Bowen et al. [2001], haze episodes are identified in 1982, 1987, 1991, and 1994 and 1997/98 by elevated TOMS AI values. The global TOMS ozone analysis of Ziemke and Chandra et al. [2002] showed that the 1997/1998 event in Indonesia was the

single largest detected change in total columnar ozone during their 1979-2000 period of analysis.

1.4. Impacts of fire and smoke in Indonesia

Local impact assessments of the fires have also focused on the 1997/98 disaster. Nichol [1998] described the impacts on transportation and shipping, including significant loss of life caused by a jetliner crash in Sumatra, cargo ship collision in the Strait of Malacca and the sinking of a passenger ferry in South Kalimantan. Arguably, the most serious local impact is the effect of prolonged exposure to haze on human health, as described for the 1997 fires in Tomich et al. [1998], Kunii et al. [2002], Sastry [2002], and Frankenberg et al. [2005]. The negative ecological impacts of the fire and haze were described in Nasi et al. [2002] and Van Nieuwstadt and Sheil [2005], along with Davies and Unam [1999] and Yoneda et al. [2000] who emphasized the reduced vegetation growth caused by smoke-haze. The economic impacts have been assessed in Menz et al. [1999], Glover and Jessup [1999] and the Asian Development Bank (ADB) [1999], who's estimate of impacts exceeding \$9 billion US has been widely referenced. The main economic losses described by the ADB were due to timber and agricultural losses, the increased risk of flooding from loss of forest cover, and the release of sequestered carbon as biomass burning emissions.

The global climatic impacts of the 1997 fires have also been examined. Liew et al. [1999]'s area burned estimates were used in a basic emissions calculation to conclude that carbon emissions from the 1997/1998 fires were an order of magnitude greater than the Kuwaiti oil fires of 1991 [Levine, 1999], similar to the result for the 1994 fires found by Nichol et al. [1997]. Also incorporating high-resolution satellite imagery, Page et al. [2002] estimated that the direct carbon emissions from the peat fires in 1997 represented between 13% and 40% of mean annual global fossil fuel emissions.

In addition to these basic estimates, several modeling experiments were performed to assess the effect of emissions from the 1997 event on the climate system. Sudo and Takahashi [2001] suggested that roughly half of the observed increase in ozone

concentration over the Western Pacific could be attributed to the Indonesian fires, primarily through lower-tropospheric effects. Hauglustaine et al. [1999] also showed that regional ozone concentrations were also highly sensitive to emissions from the 1997 Indonesian emissions, using the emissions estimates of Levine [1999] as input to a global chemical transport model. Podgorny et al. [2003] quantified the climatic impacts of the 1997 event, estimating that aerosol emissions from the fires resulted in at least a 50% increase in atmospheric solar heating within the first three vertical kilometers, and at least a 15% reduction in seasonal mean solar radiation absorbed by the equatorial Indian Ocean. Brasseur et al. [1998] estimated that biomass burning in the tropics has contributed to an increase in tropospheric ozone over the past century and a half, and that the biggest predicted increase over the 1990-2050 period will be seen in south and Southeast Asia.

1.5. Causes of fire and smoke in Indonesia

Stolle and Lambin [2003] provided a useful conceptual model of fire occurrence in Indonesia, clearly distinguishing between underlying socio-economic and natural causes. A thorough review of the socio-economic causes of the fires is given by Applegate et al. [2001], who emphasized weak regulatory capacity and ultimately, increased population in Sumatra and Kalimantan as the result of Indonesia's transmigration programs. Bowen et al. [2001] described how forest logging, conversion to agro-forestry plantations and oil and gas exploration contribute significantly to increased landscape flammability, particular in low-lying wetlands. By analysing the underlying land-tenure classification of area burned in East Kalimantan during 1998, Siegert et al. [2001] showed that increased logging and forest use has increased fire susceptibility, noting that undisturbed tropical forests are normally resilient to fire even during droughts.

With population and landscape change as the underlying causes, the 'trigger' for severe fire and haze episodes is drought. Broadly, there are two large-scale climatic phenomena which govern rainfall and drought in Indonesia: the Asian-Australian monsoon and El Niño Southern Oscillation (ENSO). The Asian-Australian monsoon refers to the shifting of wind and precipitation patterns over the Indian Ocean, South

Asia and Southeast Asia throughout the year [Hartman, 1994]. During the southwest monsoon from July to September, the Tibetan plateau is heated at the surface, drawing warm moist air northward from the Indian Ocean, and a resulting in increased precipitation over the Indian subcontinent and reduced precipitation during the dry season over Indonesia. During the northeast monsoon from November through February, the atmospheric flow is reversed, resulting in Indonesia's main wet season.

Descriptions of Indonesia's wet and dry season must be put in relative context. During a typical dry season in Indonesia, there is still sufficient rainfall to inhibit widespread fire and haze. For comparison to a wet part of Canada, Palembang in South Sumatra receives an average of 95 mm of rainfall during its driest month (July), compared to 145 mm in Victoria, BC, during its wettest month (September) (Figure 1).

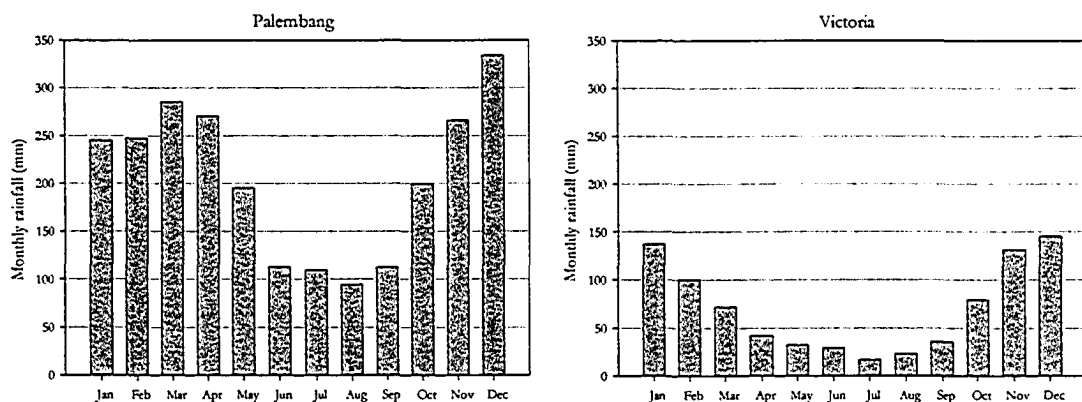


Figure 1. Monthly rainfall in Palembang, South Sumatra and Victoria, British Columbia (from the Global Historical Climatology Network)

During warm phases of the ENSO however, dry-season rainfall over Indonesia is greatly reduced, due to a change in ocean and atmospheric circulation in the tropical Pacific. The Walker circulation which characterizes the westwardly flow over the tropical Pacific is weakened, resulting in a reduced pooling of warm water and reduced convection in the western Pacific [Chandra et al, 1998; Gutman et al., 2000; Hendon, 2003]. Over Indonesia and Australia, this results in a pronounced decrease in rainfall during their respective dry seasons, as the convection shifts eastward into the

central Pacific. In fire prone regions of Indonesia, burning for agricultural and forest plantation clearing escapes control, and during severe episodes ignites vast deposits of peat which have limited water holding capacity due to extensive draining.

1.6. Historical haze indicator

The results of Levine [1999] and Page et al. [2002], as well as the related modeling studies, showed that Indonesian biomass burning has a pronounced effect on the global climate system. These studies however are limited to the 1997 event, with the longer term impacts of Indonesian biomass burning not yet examined. To do this, the first requirement is a longer term emissions inventory from Indonesia, as input to studies modeling the emissions impact on the global atmospheric chemistry. A historical haze indicator will also be useful for validation of air quality models outside of the 1997 episode, and long-term epidemiological studies of smoke impacts on human health [Bell et al., 2004]. Finally, and most closely related to the aims of this study, the haze indicator will improve attribution studies relating haze occurrence to changing population, land-cover and climate characteristics such as that by Stolle and Lambin [2003], de Groot et al. [2005], and Dymond et al. [in press], which form the basis of early warning system development.

The TOMS AI is the best indicator available for a long-term proxy of Indonesian smoke-haze compared with satellite-based fire detection and direct air quality measurements, but there are several serious problems with the sensor. There have been several changes in the mission, from the NIMBUS/7 sensor from 1979 to 1992, the METEOR-3 sensor for 1993 to 1994 and the Earth-Probe sensor from 1996 to the present. Such a change in sensor complicates any long-term analysis, in that interannual variation in TOMS AI could be due to instrument artifact. Although every effort has been made to account for these sensor changes, Kita et al. [2000] specifically analyzed the haze episodes as separate events, cautioning against any inter-annual comparison across sensor changes.

Furthermore, the TOMS AI also preferentially detects higher-altitude smoke emissions [Herman et al., 1997]. Aerosols in the boundary layer are more difficult to distinguish from noise from the earth's surface, and detection is only effective at

altitudes above 1.5 km [Hsu et al., 1999]. While high-intensity forest-fires in temperate forest can rapidly inject smoke emissions above this height [Fromm and Servranckx, 2003], the smoldering peat fires responsible for the bulk of the smoke emissions in Indonesia burn at much lower intensity, and are unlikely to immediately inject emissions above the boundary layer. This is a likely reason why the TOMS sensor failed to detect the lower-magnitude 1987 haze episode [Wang et al., 2004]. Gradual diffusion and upwards entrainment then, will be the principal mechanism through which smoke is transported upwards, if at all. Because smoke at higher altitudes has also been subject to increased vertical and horizontal advection, some smoke detected above the boundary layer will have been transported from distant sources. The TOMS data therefore may be under-representing the full magnitude of smoke emissions and are ill-suited to providing local haze characterization. Finally, any historical reconstruction of haze is limited to 1979, the beginning of NASA's TOMS mission.

1.7. Study objectives

Because of the lack of historical fire records and air quality measurements, along with the limitations of the TOMS sensor, it is desirable to have alternative indicators of smoke haze for historical analysis. Heil and Goldammer [2001] showed that visibility observations were a useful indicator of smoke haze at several sites in Indonesia during the 1997 event, compared to direct air quality measurements which were taken discontinuously for a brief period during the disaster. In the global visibility analysis of Husar et al. [2000], Indonesian biomass burning in particular appeared as a significant haze event. The analyses of Field et al. [2004] and Wang et al. [2004] subsequently provided the first multi-year applications of visibility as a haze proxy for Indonesia. Field et al. [2004] analyzed the relationship between drought and haze in Western Indonesia over the period from 1994 to 1999, showing that severe haze episodes occurred only above a given threshold of drought. Wang et al. [2004]'s longer-term analysis from 1973 to 2003 of haze in southern Sumatra confirmed the fact that major haze events occurred in concert with warm ENSO phases.

The objectives of this study are twofold:

1. To develop a proxy haze dataset for the whole of Indonesia including Kalimantan, extending the long-term analysis for Sumatra by Wang et al. [2004]. A haze dataset covering Sumatra and Kalimantan is expected to form the basis of future proxy emissions studies, required to extend the global atmospheric chemistry modeling studies described above back over a longer analysis period.
2. To examine drought as a causal factor of the haze in different regions, extending the short-term analysis of Field et al. [2004]. Such an analysis has significant operational importance, as knowing what level of drought is associated with severe haze is a key component of any haze disaster early warning system. Several different drought indices will be assessed according to their predictive power, ranging from simple cumulative precipitation indices to more sophisticated soil moisture models. Special attention will be given to the problem of estimating a threshold of moisture below which haze events have historically occurred.

The remainder of this thesis is organized as follows. Chapter 2 describes the sources of visibility and drought data, as well as two auxiliary datasets used to select appropriate domains for the drought-haze analysis. Chapter 3 describes the methodology used to process the visibility and drought data, and the statistical techniques employed to describe the relationships between drought and haze in Sumatra and Kalimantan, and estimate drought threshold levels. Chapter 4 summarizes results from the visibility dataset reconstruction and drought analysis. Chapter 5 discusses implications of the results in terms of the relative magnitude of past events, early warning of future haze disasters, and areas for further research.

2. Data

2.1. Visibility data

Visibility is a primary meteorological parameter having two functions: as an air mass descriptor in synoptic meteorology, and for purposes of aviation. Jacobson [2002] defines visibility as a measure of how far we can see through the air. More formally, the World Meteorological Organization (WMO) distinguishes between nighttime and daytime visibility [WMO, 1996]. Meteorological visibility by day is defined as “the greatest distance at which a black object of suitable dimensions, located near the ground, can be seen recognized, when observed against a scattering background of fog, sky, etc.” For practical observation purposes, meteorological visibility at night is defined as “the greatest distance at which lights of moderate intensity can be seen and identified”.

WMO [1996] provided a detailed description of visibility observing procedures and related physical quantities. Visibility observations are measured in increments proportional to their magnitude: in 100m steps between 100m and 5000m, in steps of 1km between 6km and 30km, and steps of 5km between 30km and 70km. Visibility observations can be made using natural or man-made objects at known distances used as landmarks. Meteorological stations prepare plans of landmarks and their distances from the station, including objects suitable for day and nighttime observation. Figure 2 shows an example visibility observing plan for Kuala Lumpur in Malaysia, for the medium range visibility scale. Observations are made without the aid of optical devices such as binoculars or telescope and are taken at ground level.

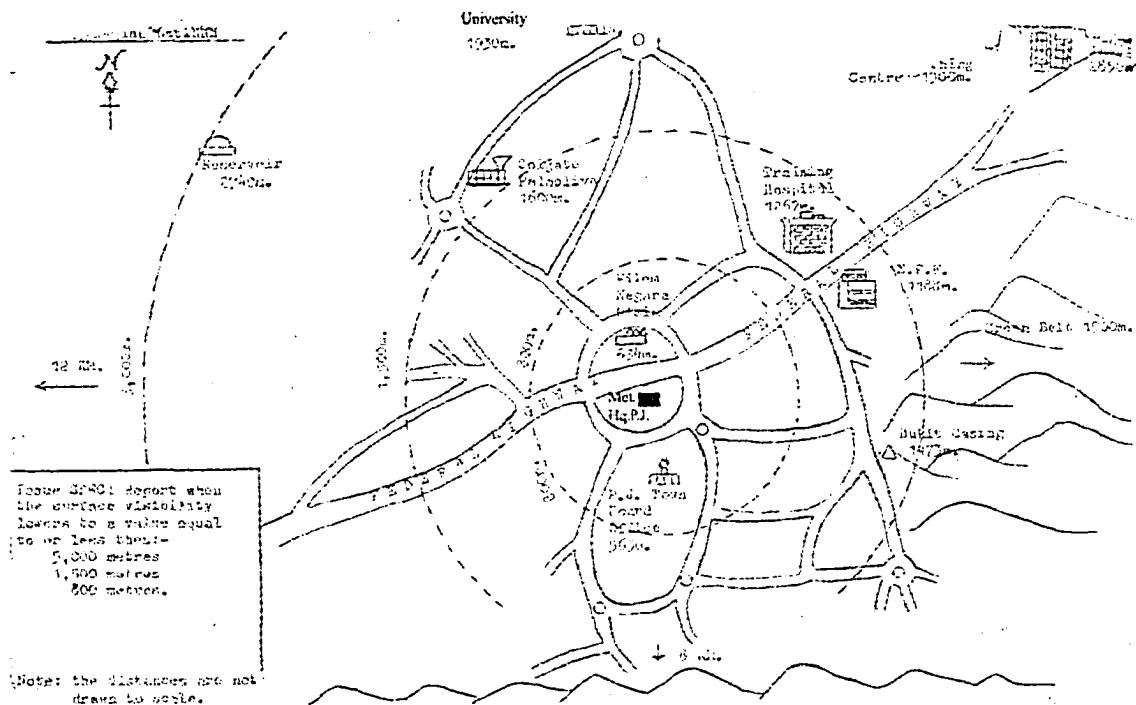


Figure 2. Medium-range visibility observation contours for Kuala Lumpur, Malaysia (from M. Mohamad, Malaysian Meteorological Service)

The physical quantity being measured is the meteorological optical range, the length of path in the atmosphere required to reduce the luminous flux in a straight beam from an incandescent lamp to 5% of its original value. The factor by which meteorological optical range is reduced over a given distance is the extinction coefficient, formally defined as the degree to which light is attenuated over a straight path due to scattering and absorption by particles and gases in the atmosphere. Total extinction coefficient represents the sum of extinction coefficients from all contributing gases and particulates, from both scattering and absorption. Note that rainfall and fog also affect visibility, and therefore, any use of visibility observations as a haze indicator must account for this.

Scattering by particles in the atmosphere is primarily responsible for visibility reduction, rather than absorption or gaseous scattering [WMO, 1996; Jacobson, 2002]. Specifically, it is accumulation mode particles (diameter between 0.1 and 2 μ m) which most strongly affect visibility, as their size range corresponds most closely to that of visible light wavelengths. Biomass burning hence reduces visibility

primarily through its emissions of particulate matter, rather than gaseous emissions. The most important constituents from biomass burning relevant to visibility and extinction coefficient, in terms of both scattering effect and relative emissions quantities, are ash, organic matter and soot (black carbon) [Jacobson, 2002].

2.1.1. Previous applications of visibility observations

Compared to other meteorological parameters, visibility is relatively subjective and depends upon the perceptive and interpretative ability of the observer, and characteristics of the landmarks used for distance estimation. Visibility is though, the most widely available meteorological indicator of atmospheric pollution, and has therefore been used extensively as a historical and proxy indicator in air pollution studies.

In several studies, visibility observations have been used as a long-term indicator of haziness, often used to determine the effects of temporal changes in emission patterns of industrial pollution. Husar et al. [1981] analyzed visibility observations in the eastern US, and found that the substantial visibility decrease in the Smoky Mountain region from 1948 to 1974 region was consistent with an increase in coal consumption. In their update of this study, Schichtel et al. [2001] saw a reversing of this trend, with the visibility increase over the same region corresponding to an overall decrease of sulfur emissions, a major pollutant from coal burning. Doyle and Dorling [2002] analyzed visibility observations for eight stations in the UK, noting that decreases in haziness in Britain in 1973 corresponded to reduced fuel consumption during the oil crises of that period, and that the subsequent long-term decline for most stations' haziness was due to the introduction of catalytic converters and improved fuel efficiency in automobiles. Qian and Giorgi [2000] observed decreasing trends in visibility over the Sichuan Basin China since the 1970's, which they thought to be caused by increased emissions of SO₂ as a result of rapid industrialization in the province. In a related study, Kaiser and Qian [2002] attributed decreases in sunshine duration over eastern China and a decrease in daily maximum temperature in the Sichuan Basin to increased atmospheric aerosol loading as measured by visibility observations. In all of the above studies, changes in visibility have been linked to

certain underlying factors. Visibility observations have also been used as a proxy for particulate matter in epidemiological studies, given that the former has far greater sampling frequency because of its inclusion in synoptic meteorological reports [Delfino et al., 1994; McDonnell et al., 2000; O'Neill et al., 2002; Tsai et al., 2003].

The recent study of Husar et al. [2000] analyzed global daily mean visibility for 7000 weather stations from 1994 to 1998, showing the global variation in visibility, with pronounced seasonal variation in sub-Saharan Africa and western Indonesia. In sub-Saharan Africa, visibility reached its lowest values during the December, January, February period. In Duncan et al.'s [2003] analysis of global fire emissions, there is also a pronounced increase in biomass burning emissions in this region (see their Figure 5) during the same months. A similar comparison for Indonesia also shows that the minimum period of visibility and of maximum biomass burning emissions are both during the June through September dry season. Because Husar et al. [2000] excluded days with elevated fog or significant precipitation, seasonal decreases in visibility would appear consistent with a corresponding increase in biomass burning in these two regions.

Brauer and Saksena [2002] also noted that visibility observations were an appropriate indicator of particulate emissions from forest fires. Specifically in Southeast Asia, Yadav et al. [2003] found a significant relationship between particulate matter and visibility in Brunei during the 1998 haze episode, which was in part due to transboundary forest fire emissions from East Kalimantan.

2.1.2. Description of synoptic meteorological data collection in Indonesia.

Indonesia's primary meteorological network spans the entire archipelago and operates according to guidelines of the World Meteorological Organization (WMO). Stations are located primarily at airports of major cities, as is typical of most WMO-class stations, with higher station density over the heavily populated island of Java (Figure 3). Following WMO requirements, observations are made every 3 or 6 hours, referred to as 'synoptic' reporting times. Despite this comprehensive data collection program, digital archives in Indonesia are lacking [Page et al., 2004], and hardcopy records exist primarily at individual stations. The cost of retrieving, cataloguing and

digitizing these records was prohibitive for this study, although a concerted data recovery effort is underway with cooperation from NOAA and other international donors (M. Ratag, pers. comm.).

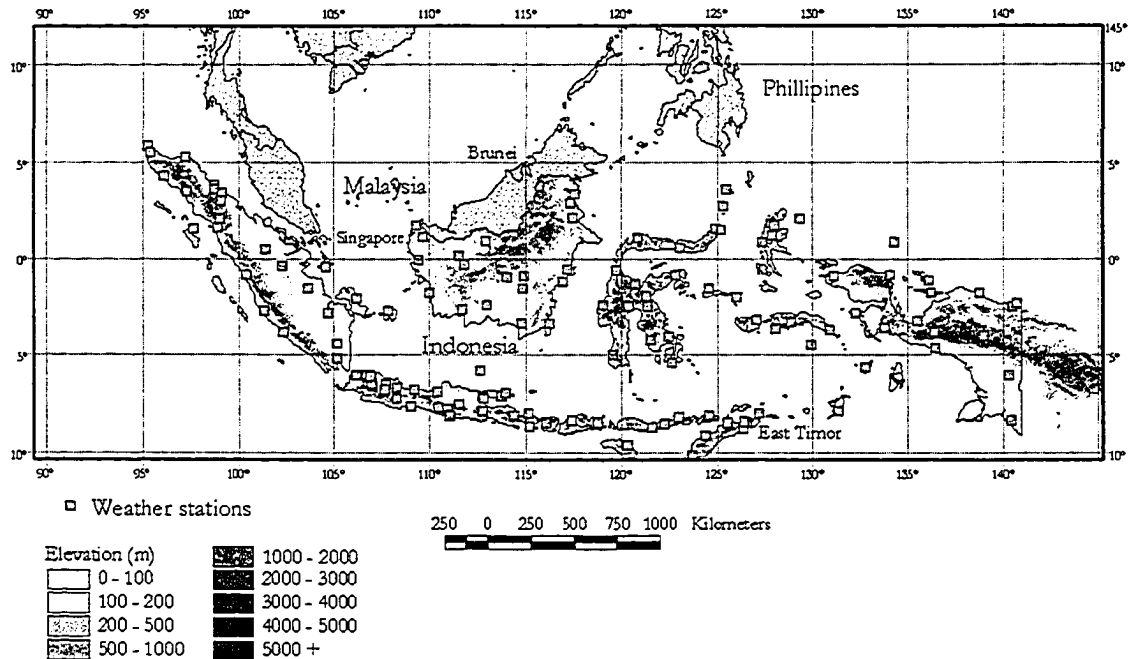


Figure 3. Weather station distribution over Indonesia

Synoptic records were therefore obtained for the network via National Oceanic and Atmospheric Administration's (NOAA) National Climate Climatic Data Centre (NCDC), who archive synoptic records as they are transmitted through the Global Telecommunications System (GTS). In total, data were available for 176 weather stations from the NCDC's Integrated Surface Hourly (ISH) dataset. Each record contains two types of information: station metadata, including unique station identifier, elevation, geographic coordinates, and observation time, and weather parameters such as temperature and wind speed [NCDC, 2003].

For the purposes of this visibility analysis, four of the 43 available meteorological parameters were used: visibility, dry-bulb temperature, dew point, and present weather codes. The present weather codes are pre-defined qualitative descriptors describing the prevailing weather conditions at the time of observation. There are 100

present weather descriptors available, 80 of which are used to describe different types of rainfall or fog conditions.

2.2. Moisture indices

Drought definitions vary geographically and according to the effects under consideration [American Meteorological Society 1997; Heim, 2002]. Meteorological or climatological drought is defined as the set of atmospheric conditions resulting in the absence or reduction of precipitation, and is a strictly physical definition. Agricultural drought assesses the characteristics of meteorological drought on crop growth, and is usually measured in terms of soil moisture deficiency. Hydrological droughts are concerned with the effects of reduced rainfall on water supply, and usually lag behind meteorological drought. Socio-economic drought reflects the impacts of meteorological, agricultural and hydrological drought on a broader range of societal factors.

In the context of biomass burning and haze, drought takes on aspects of each of the above definitions, and so indices were selected to reflect these different aspects. Meteorologically, severe fires in Indonesia have occurred during abnormally dry years, induced by the warm phase of the ENSO. Agriculturally, fire and smoke activity is not directly related to plant growth, but rather to the moisture content of dead and live vegetation. Hydrologically, fire and haze in Indonesia is largely governed by the moisture content and water table height in vast peatlands, which have been converted into agricultural and forest plantations and where the most severe burning occurs. As described above, the most significant impacts of fire-related drought are socio-economic. Indonesian fire emissions also reflect a unique aspect of drought impact, because of the substantial effect on the global climate system.

A drought index is defined as “an index which is related to some of the cumulative effects of a prolonged and abnormal moisture deficiency.” [WMO, 1992]. The analysis of Field et al. [2004] examined the relationship between drought and haze over the period from 1994 to 1999, using the publicly available Global Summary of the Day (GSOD) data from the NCDC. In that study, the Canadian Fire Weather Index System Drought Code (DC) was computed from the GSOD data, and compared

to daily visibility to estimate a drought threshold above which the 1994 and 1997 episodes occurred. The result was a new DC classification system appropriate for Indonesia, which is now being used operationally by the Indonesian Bureau of Meteorology and Geophysics, in Malaysia by the Malaysian Meteorological Service and by the Association of Southeast Asian Nations for all of Southeast Asia as part of their operational fire danger rating systems. A similar moisture index was used by de Groot et al. [2005] to examine the relationship between weather conditions and moisture content of dead surface fuels, and by Dymond et al. [in press], in analysing hotspot occurrence according to modelled fuel moisture.

The DC requires daily observations of temperature and rainfall for computation, and is essentially a simple model of moisture content in deep organic soils. Preliminary examination of the ISH dataset showed that long-term observations of hourly rainfall were too incomplete to be totaled as daily values for computation of the DC, and no other available sources of daily rainfall data were available prior to 1994. Missing rainfall data are particularly problematic for DC computations, as a single missing observation when substantial rainfall occurred introduces significant bias towards higher DC values. This is especially true in the tropics, where isolated days of rainfall exceeding 100mm are not uncommon.

The analysis of drought and haze was therefore limited to monthly values, for which extensive moisture data are available. For a longer-term study, it was also appropriate to focus on lower-frequency variations in drought and haze. Four indices were selected for the analysis, reflecting the different aspects of drought, and the availability of different data products, to determine which was the best predictor of severe haze. The indices ranged from simple cumulative precipitation totals to more sophisticated soil moisture models, and are described below. For simplicity, the indices will be referred to collectively as moisture indices.

2.2.1. Chen et al. [2002] PRECL dataset

The simplest moisture index was derived from the global rainfall dataset of Chen et al. [2002], from the National Centre for Environmental Prediction (NCEP), known as

PRECL, referring to precipitation over land. Data are blended from several different source datasets from 1948 to the present. The main source of data for the period from 1948 to 1975 is the Global Historical Climate Network (GHCN), with observation counts increasing from 1948, and peaking in 1970. After 1976, non-redundant stations from the Climate Anomaly Monitoring System (CAMS) were added to account for less GHCN data. The CAMS data are closely related to the synoptic observations from distributed globally in real time through the GTS. In Indonesia, these data are largely derived from the same synoptic network containing the visibility observations. CAMS data represents the majority of the observations in the dataset after 1981. Between the two GHCN and CAMS datasets, the PRECL dataset contains over 17000 unique rainfall stations globally.

Data undergoes significant quality control, using the exhaustive algorithms of the Global Precipitation Climatology Centre (GPCC) operated by Germany's National Meteorological Service. Station meta-information is checked to ensure the accuracy of station location and elevation, and actual rainfall data are checked automatically for coding error, spatial homogeneity and highly anomalous values, with flagged data inspected by hand and cross-checked with other data sets and with consideration given to local orographic effects. Also, observation error is thought to be greatest at northern latitudes due to historical under-catchments of snowfall, and so Indonesia is expected to have relatively little observation error for precipitation.

Data were gridded to a 2.5° by 2.5° resolution, which corresponds roughly to a distance of 275km between grid cell centers at the equator, the approximate centre of the analysis domain. Significant consideration was given by Chen et al. [2002] to the interpolation algorithm used for data gridding. Four different algorithms were compared using data-hiding techniques, each applied to datasets of raw values and mean centered anomaly data. Their comparison showed that a covariance-based optimal interpolation method using mean-centered anomaly data provided the best results, in terms of correlation, minimal root-mean squared error and minimal bias. This was particularly the case for Indonesia, which constituted a special validation case in their study. In terms of a strict gauge-derived rainfall dataset then, PRECL is considered to be the best available source with coverage over Indonesia.

2.2.2. Adler et al. [2003] GPCP dataset

A second rainfall dataset was the Global Precipitation Climatology Project (GPCP) rainfall dataset [Adler et al., 2003], the result of a significant multi-institutional effort involving NASA, NOAA and the University of Maryland. The GPCP differs from NCEP's PRECL dataset in that it incorporates both gauge-based surface observations and satellite data. The dataset has a 2.5° by 2.5° spatial resolution, and spans the period from 1979 to present, with the shorter length of record owing to the recent availability of satellite data.

The gauge data used was similar to that of Chen et al. [2002], incorporating data from both the GHCN and CAMS source datasets, and also the quality control algorithms of the GPCC. Microwave and infrared sensors were used, the full details of which are given by Adler et al. [2003]. The incorporation of satellite data has been shown to improve the accuracy of gridded rainfall fields, particularly over regions with sparse surface gauge density [Gebremichael et al., 2003], and so was warranted for inclusion in this analysis as a comparison with the strictly gauge-based dataset of Chen et al. [2002]. Furthermore, efforts are currently underway to incorporate operational remotely-sensed rainfall data into operational fire danger rating systems in Indonesia [O. Roswintiarti, pers. comm].

2.2.3. Fan and van den Dool [2004] SOILM dataset

In addition to the two rainfall datasets, the National Centre for Environmental Prediction global 'Leaky Bucket' soil moisture (SOILM) dataset of Fan and van den Dool [2004] was also used. When calibrated to different soil types and climates, this type of soil moisture model would be a basic component of any agricultural drought monitoring program at a global scale, given that direct soil moisture monitoring at a global scale would be cost prohibitive.

Because of the relevance of soil moisture to biomass burning, most fire danger rating systems include models for soil moisture, including the Canadian Forest Fire Danger

Rating System and the National Fire Danger Rating system in the US. The Drought Code used in Field et al. [2004], for example, is essentially a soil moisture index, measuring the moisture content of deep compacted organic soils such as peat. Given the accessibility of the SOILM dataset, it was therefore useful to examine the relationship between a more sophisticated soil moisture model and haze occurrence, with respect to a simple rainfall-based index.

The basic premise of the SOILM model is to describe the change in soil moisture w as the difference between moisture input through precipitation P and output through evapotranspiration E and runoff R

$$\frac{dw}{dt} = P - E - R.$$

This is a largely empirical single layer model, with model parameters tuned to field studies in the US Great Plains, and with no parameter variation across soil or landcover types, though work is currently underway to calibrate the model to different soil types and climates. As input, the model uses the monthly precipitation data of Chen et al. [2002], and surface temperature data from the NCEP Reanalysis dataset [Kalnay et al., 1996]. Data are distributed at a 0.5 by 0.5 spatial resolutions, and available for 1948 to the present. The units are in millimeters of stored precipitation, but should only be considered on a relative scale outside of the US, given the lack of calibration in other regions.

2.2.4. Dai et al. [2004] PDSI dataset

The last index considered was the Palmer Drought Severity Index (PDSI), computed globally by the National Centre for Atmospheric Research [Dai et al., 2004]. The PDSI was designed mainly for agricultural applications to measure the cumulative departure in moisture supply and loss at the surface, but has been applied in numerous other applications, including historical forest fire and climate analyses [Hessl et al., 2002; Westerling et al., 2003; Hessl et al., 2004]. It is an anomaly-based index, in that local means of rainfall are included as moisture parameters. It is also a cumulative index, with the current month's PDSI a function of the current month's weather and last month's PDSI.

The PDSI uses a two-layer soil model, with all precipitation directly available for absorption. This is known to complicate model calculations at latitudes with a distinct winter season, but was presumed to not be a problem in the tropics. Unlike the SOILM model, the PDSI model does distinguish between the water holding capacity of different soil types globally. PDSI values are on a standardized scale, with a minimum of -10 corresponding to severe moisture deficit and a maximum of +10 corresponding to a moisture surplus. The technical details of the PDSI are described in Palmer [1965], with an accessible summary given by Ntale and Gan [2003]. Unlike the SOILM model, the PDSI has undergone some validation against field data outside of the US, in particular showing strong correlation with measured soil moisture in southern China and streamflow in Brazil and the Congo, particularly compared with raw rainfall measurements [Dai et al., 2004], despite being designed primarily for semiarid environments [Heim, 2002].

2.3. Land cover for peat identification

For analysis of the drought and haze relationships in Sumatra and Kalimantan, stations were selected in part based on proximity to peatlands. The World Wildlife Fund (WWF) Terrestrial Ecoregions of the World Map [Olson et al., 2001] was used to identify peat areas. Four of the WWF categories were classified as peatlands: Sunda Shelf peat swamp forest, Southwest Borneo freshwater swamp forest, Sumatra freshwater swamp forest and Sumatra peat swamp forest. For the purposes of this study, the relevant peatlands are in South Sumatra, Jambi and Riau province of Sumatra, and Central Kalimantan.

2.4. Wind streamlines from Reanalysis data

The NCEP Reanalysis [Kalnay et al., 1996] was also used to assess the atmospheric flow over Indonesia responsible for smoke transport. The Reanalysis represents an exhaustive assimilation of meteorological data, containing a full three-dimensional characterization of the atmosphere at 6-hour temporal resolution from 1948 to the

present. Included in the Reanalysis are wind fields at 28 vertical levels, which were used to compute monthly average 850 mb wind fields, used subsequently to determine the predominant direction of atmospheric flow during the dry season months. The Reanalysis dataset also contains surface precipitation as a parameter, and was hence considered for inclusion as a candidate moisture index. Kalnay et al. [1996] caution that the Reanalysis rainfall data are categorized as an entirely derived 'Type 3' variable, and hence should not be used directly for hydrological analysis, and was therefore not included in the comparison of moisture indices.

3. Methods

3.1. Visibility dataset development

3.1.1. Preprocessing

Data obtained from the NCDC was stored in an encoded format, requiring several pre-processing steps. All records with missing station location information were discarded, as were all duplicate entries with different observation values, as there was no way to identify the actual observation value with any certainty. Relative humidity is a key parameter for data filtering, but was not available directly in the observations, and so was calculated from the dry-bulb and dew point temperatures according to a modified version of the Clausius-Clapeyron relationship.

3.1.2. Hydrometeor filtering

Visibility is affected not only by atmospheric pollutants, but also by naturally occurring precipitation and humidity, referred to as hydrometeors. To obtain a meaningful indicator of haze, it was necessary to filter out records where decreased visibility could not be attributed exclusively to smoke-haze. To eliminate fog effects, all observations were excluded where the relative humidity was greater than 90%, according to the filtering rules of Husar et al. [2000] and Doyle and Darling [2002]. Also, observations whose present weather codes identified the presence of precipitation or fog were also excluded. For fog conditions, an exception was made if the relative humidity was less than 75%. Husar et al. [2000] describe these as 'dry fog' conditions, where reduced visibility is not likely due to hydrometeorological factors, describing Indonesian biomass burning as a specific reference case. Both studies also excluded observations having a non-negligible precipitation total. After initial inspection of the synoptic records though, it was determined that rainfall observations were too incomplete to be used in this way.

3.1.3. Extinction coefficient calculation and monthly statistics

It is standard practice to convert visibility values to their equivalent extinction coefficient in any historical or comparative study [Qian and Giorgi, 2000; Husar et

al., 2000; Schictel et al., 2001]. Extinction coefficient B_{ext} was computed using the Koschmeider relationship

$$(1) \quad B_{ext} = \frac{K}{V}$$

where K is the Koschmeider constant and V is the visibility. The Koschmeider constant K corresponds to the contrast sensitivity threshold of the observer and the inherent contrast between visibility targets and the background sky. Different values of K have been determined from empirical studies, but a value of $K=1.9$ was chosen, according to the more recent studies of Husar et al. [2000] and Schictel et al. [2001]. Initial inspection of the data showed that visibility could take on a minimum value of 0, corresponding to periods when visibility was completely obscured, which does not allow for calculation of B_{ext} . During non-hydrometeorological events, these observations correspond to severe haze, and so were important to include for the sake of measuring the full magnitude of severe haze events. Therefore, 0-valued visibility was assigned a value of 100m, the smallest non-zero value for which haze is reported in the dataset.

To create a lower-frequency dataset, the mean, variance, quartiles, and median of all synoptic B_{ext} values were calculated for each month over all synoptic hours, similar to the annual averaging done by Qian and Giorgi [2000]. The number of valid observations for each month was totaled as was the number of monthly observations screened in through the hydrometeor filters. B_{ext} values were also log-transformed to reduce the skewness of the monthly distributions. These station-wise monthly summary statistics are the product to be released as a publicly available dataset through the NCDC.

3.2. Drought and haze analysis

3.2.1. Regional signals for Sumatra and Kalimantan

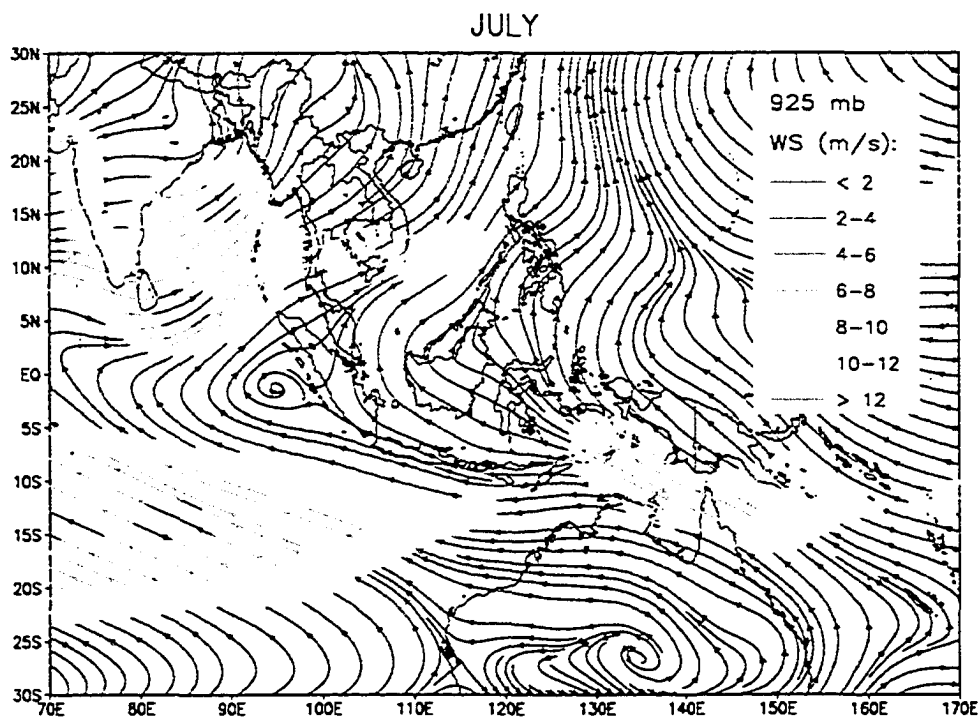
The relationship between drought and haze was focused on Indonesia's most fire prone regions, the peat lands of Sumatra and Kalimantan. [Nichol, 1997;

Hauglustaine, 1999; Heil and Goldammer, 2001; Ikegami et al., 2001; Page et al., 2002]. Monthly regional moisture and haze signals were computed over a sub-domain of each island, corresponding to the areas with the most severe burning. A similar approach was used successfully by Field et al. [2004], who computed a single regional signal over the relevant areas of Sumatra and Kalimantan, by averaging daily values of moisture and haze across stations. Qian and Giorgi [2000] also averaged B_{ext} values across multiple stations in their trend analysis of haze over the Sichuan Basin in China. Partitioning the analysis domain between Sumatra and Kalimantan was expected to preserve any inter-regional variability between the two domains.

The moisture domains for Sumatra and Kalimantan consisted of $5^{\circ} \times 5^{\circ}$ bounding boxes, each containing 4 grid cells for the 2.5° resolution PRECL, GPCP, and PDSI datasets, and 100 grid cells for the 0.5° resolution SOILM datasets. For each month, moisture values were averaged across the cells in the domain to obtain monthly regional moisture signals, similar to the averaging of monthly rainfall across stations by Hendon [2003]. Selection of these domains was a balance between including the relevant emissions, while excluding areas without substantial biomass burning. Although there is a substantial portion of ocean in each domain, the rainfall and moisture datasets are limited to land-based observations for the three non-satellite based moisture datasets, and so primarily reflect conditions on land. As discussed above, drought is a cumulative phenomenon, and in this case evolves over several months of anomalously low rainfall. Therefore, a 3-month backward moving total of rainfall was computed and used as the moisture index derived from the PRECL and GPCP datasets.

Visibility stations in each analysis domain were selected based on data completeness and their proximity to the peatlands of interest, with consideration given to the direction of atmospheric flow during the dry seasons and the effect of topography. During the southwest monsoon dry-season months from July through September, flow over Sumatra and Kalimantan is from the southeast (Figure 4). In total, 4 stations were included in the haze signal for Sumatra and 6 stations were included for Kalimantan (Table 1, Figure 5). In Sumatra, the most intense area of burning is in the low-lying coastal region of South Sumatra, extending northward along the coast into

the southern half of Riau province [Heil and Goldammer, 2001; Bowen et al., 2001], corresponding to the most intense area of transmigratory resettlement, land conversion and peat swamp draining. Two stations outside of the moisture domain were selected, Pekanbaru (961090) and Rengat (961710), both in Riau province. Although less intense than in Jambi and South Sumatra, burning does occur in Riau and the stations were considered close enough downwind to the main burning areas to warrant inclusion. Two stations along Sumatra's west coast at a similar distance from the peat area as the Riau stations were excluded due to potential topographical effects, as the stations were located on the lee side of the Bukit Barisan range, with respect to the main burning area and the northeasterly flow during the dry season. Stations were selected similarly in Kalimantan, with the station in Pontianak (965810) included because of its close downwind location to the main burning area in Central Kalimantan. Two stations within the domain were excluded because they had a negligible length of record.



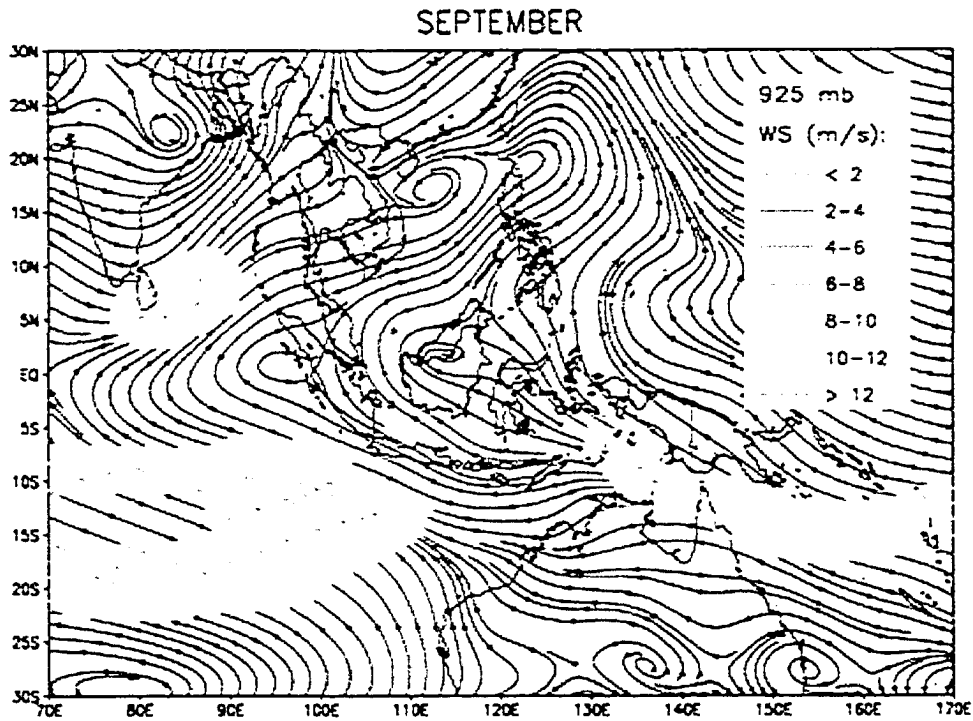


Figure 4. Average wind streamlines during the start of the dry season in July (top) through to the end of the dry season in September (bottom), courtesy of O. Roswintiarti.

	WMO ID	Name	Latitude	Longitude
Sumatra				
	961090	Pakanbaru	0.46	101.45
	961710	Rengat	-0.46	102.31
	961950	Jambi	-1.63	103.65
	962210	Palembang	-2.90	104.70
Kalimantan				
	965570	Nangapinoh	-0.35	111.78
	965810	Pontianak	-0.15	109.40
	965950	Beringin	-0.95	114.90
	966450	Pangakalanbun	-2.70	111.70
	966550	Palangkaraya	-1.00	114.00
	966850	Banjarmasin	-3.43	114.75

Table 1. Selected analysis stations for Sumatra and Kalimantan

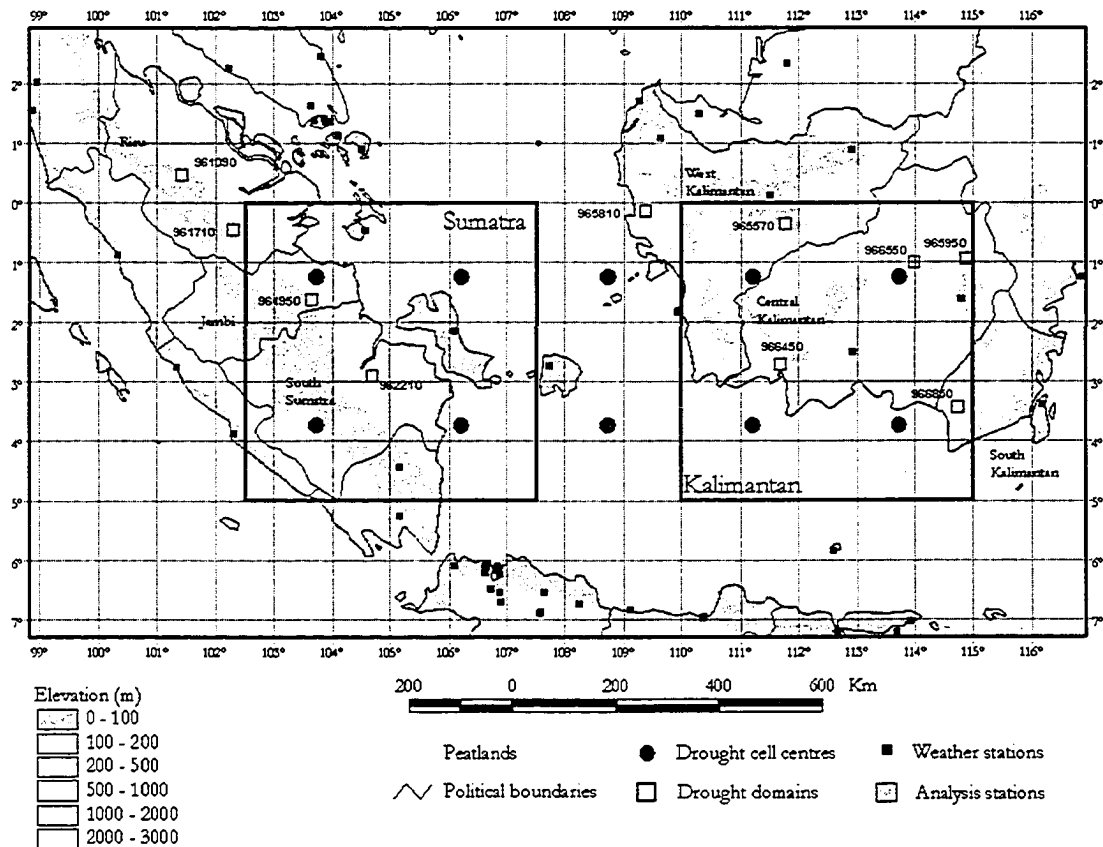


Figure 5. Visibility stations selected for analysis in Sumatra and Kalimantan, and corresponding moisture analysis domains

3.2.2. Regression and threshold analysis

Although there is a regular wet and dry season cycle driven by the Asian-Australian monsoon, it is only during anomalously dry years that fires become a serious problem. Field et al. [2004] showed this to be the case over the short period from 1994 to 1999, when there were severe haze events during the dry seasons of the 1994 and 1997 El Niño years, but a complete absence of haze events during the other non El Niño years. Their analysis showed that the absence of haze during non El Niño years corresponded to a moisture threshold above which conditions are too wet to support extensive biomass burning and haze.

Presumably, this threshold corresponds to a moisture threshold in vegetation and organic soil, which is supported by experimental data. Frandsen [1997] found this to be the case in a series of experimental burns for different organic soils across North

America, showing that the probability of ignition increases below a moisture content of 120% for the majority of soil types, and with a higher threshold for soil types with a higher inorganic content. In Indonesia, de Groot et al. [2005] showed that dead ‘alang-alang’ grass, a key surface fuel type leading to subsurface fires, had a moisture content ignition threshold of 27.8%, with field studies currently underway to estimate a similar threshold for Indonesian peatlands [W.J. de Groot, pers. comm.].

In developing an empirical relationship between moisture and haze, several statistical approaches involving some type of threshold value were considered exclusively, described in the following sections. A useful threshold represents a level of moisture below which haze events become substantially more probable. Where possible, confidence intervals for the threshold values were estimated using non parametric bootstrap methods. The drought-haze analysis was limited from 1979 to 2003 inclusive, the period over which the visibility and all moisture indices were available.

3.2.2.1. Change-point model

The simplest regression model examined was the change point regression model, also known as breakpoint, segmented, piecewise or multiphase regression. The general idea, described in detail by Seber and Wild [1989], is to model the above and below threshold partitions of the data with two regression models, constrained to be equal at an unknown changepoint, which is used as the threshold value in this context. Using the formulation of Toms and Lesperance [2003], the model is given by

$$(2) \quad f(x) = \begin{cases} \beta_0 + \beta_1 x & , \quad x \leq \alpha \\ \beta_0 + \beta_1 x + \beta_2 (x - \alpha) & , \quad x > \alpha \end{cases}$$

where α is the changepoint to be estimated, β_1 is the slope of the line below the changepoint and $\beta_1 + \beta_2$ is the slope of the second line and x is a given moisture index, and $f(x)$ is $\ln(Bext)$. This formulation constrains continuity between the two model sections at α . Under this parameterization, the significance of the change point is determined by a significantly non-zero β_2 estimate. The model was estimated through straightforward use of non-linear fitting routines.

To estimate a confidence interval for α , Toms and Lesperance [2003] suggest using an inverted F -test approach and a semi-parametric bootstrap method. Neither approach was deemed applicable for this analysis, given the assumptions regarding constant error variance and lack of error in the predictor variable in both methods. Therefore, a fully non-parametric bootstrap method was used instead, as suggested by Neter et al. [1996] and Efron and Tibshirani [1998] and Nicholls [2001]. Using this method, the random samples of pairs (x_i, y_i) are drawn with replacement from the original sample, rather than re-sampling the residuals, which is more sensitive to the underlying distribution of error terms [Efron and Tibshirani, 1998]. The changepoint function (2) is fit to each random sample, yielding a distribution of $\hat{\alpha}$ estimates. A 95% confidence interval for $\hat{\alpha}$ is obtained from the 2.5th and 97.5th percentiles of the bootstrapped distribution of $\hat{\alpha}$. For each moisture index and region, a total of 1000 resamples were drawn. As can be the case iterative estimates for nonlinear models, the numerical estimation failed to converge in some bootstrap cases, which was also considered in evaluating the moisture indices. Toms and Lesperance [2003] suggested using a smoothed parameterization of (2) to improve model fitting.

3.2.2.2. Sigmoidal model

The second model used was a simple sigmoidal curve, similar to that used in Field et al. [2004], which was found appropriate for the threshold-driven relationship between moisture and haze. The sigmoidal model is more physically realistic than the changepoint model in that it models the transition from below to above threshold conditions as a gradual transition, rather than an abrupt switch.

The selected 3-parameter sigmoidal function models the extinction coefficient by

$$(3) \quad f(x) = \frac{A}{1 + \exp\left(\frac{-(x - x_0)}{B}\right)}$$

where x is a particular moisture index, A controls the vertical scale and orientation, B controls the horizontal scale and ‘sharpness’ of the sigmoid and x_0 is the midpoint of the curve. For each of the four moisture indices compared, values decrease as drought

evolves, and so $f(x)$ is expected to increase with decreasing moisture index. In one sense, use of the sigmoidal curve can be considered as large-scale, regional analogue to the site-level analyses of Frandsen [1997] and de Groot et al. [2005], who used logistic models in their analysis of fuel moisture and ignition probability. The model was fit using the nonlinear least squares routine in SPLUS, which is based on the Gauss-Newton method.

To estimate the threshold, the gradient properties of the fitted model were examined, following Field et al. [2004]. A point on the curve was sought that represented a useful transition point from non-haze to haze conditions. To illustrate the behavior of equation (3), an example curve with its first two derivatives is shown in Figure 6. In simple terms, the first derivative represents the ‘speed’ at which B_{ext} is changing with moisture, and the second derivative its acceleration. The maximum of $f'(x)$ represents the transition point between below and above threshold conditions, and occurs at x_0 . It has little value as an early warning threshold though, as it represents a moisture level long after which the onset of a haze episode will have commenced. The second derivative represents the acceleration of the curve, and its rightmost maximum provides a useful threshold of moisture. This value represents the point after which haze increases rapidly with decreasing moisture, at $x=240$ in Figure 6. Even then, this value could possibly underestimate the threshold value; inspection of $f'(x)$ in Figure 6 indicates that the curve begins its transition to drought conditions somewhere between $x=250$ and $x=350$. Use of this gradient-based definition of drought was therefore carefully considered against values from other estimation techniques. To estimate a confidence interval for the threshold under the sigmoid model, the same paired bootstrapping approach as under the change-point model was also used.

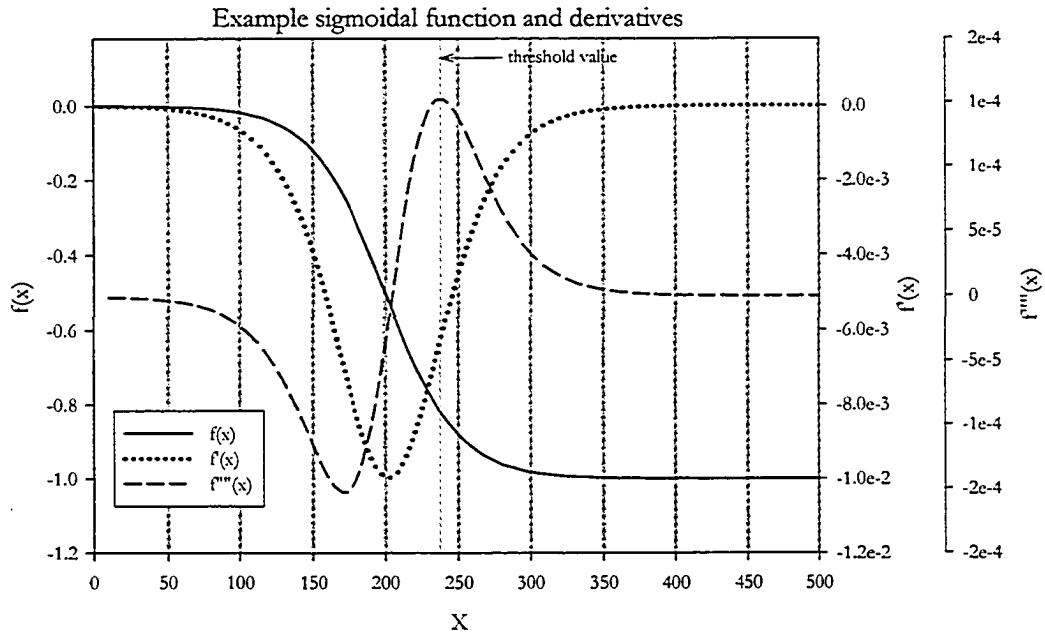


Figure 6. Example sigmoidal curve with first and second derivatives with $A = -1$, $B = 25$, and $x_0 = 200$.

It should be noted that several models similar to equation (3) were compared with respect to their flexibility and applicability to both regions and for different moisture indices. The four-parameter curve used in Field et al. [2004] and de Groot et al. [2005] was considered first, but was found to not consistently converge for several of the moisture indices, and yielded low convergence rates during the bootstrap-based threshold estimation. Several remedial measures were taken, such as rescaling the variables, using a variety of starting values and several alternative parameterizations, but all four-parameter curves considered were deemed too complex for application across regions and moisture indices.

3.2.2.3. Adaptive logistic basis functions

The third approach was the Adaptive Logistic Basis (ALB) regression of Hooper [2001], which offers a high degree of flexibility in the shape of the curve. The main strength of the ALB model over the sigmoid model is flexibility and consequent ability to capture possibly different functional relationships between each of the moisture indices and B_{ext} . Hooper [2001] illustrates the ALB's ability to model three very distinct bivariate relationships: heigh/weight ratio as a function of age in

preschool boys, nursing time of a beluga whale calf over time, and expired ventilation as a function of oxygen uptake in an analysis of anaerobic thresholds during an exercise test. Under the ALB model, the fitted model is constructed from a linear combination of logistic basis functions, and so forms a somewhat natural extension to the simpler 3-parameter sigmoidal curve. The ALB model approximates a function $f(x)$ by

$$(4) \quad \hat{f}_K(x) = \sum_{k=1}^K \delta_k \phi_k(x)$$

where K is the number of basis functions, each of which is given by

$$(5) \quad \phi_k(x) = \frac{\exp(\alpha_k + \vec{\beta}_k \vec{x})}{\sum_{m=1}^K \exp(\alpha_k + \vec{\beta}_k \vec{x})}$$

The δ_k coefficients provide the basis function weighting, and each pair of α_k and $\vec{\beta}_k$ provide the logistic basis function parameter estimates. The quantity to be minimized is the adjusted training risk

$$(6) \quad R_{GCv}(\hat{f}_K) = \left(\frac{n}{n-p} \right)^q \frac{1}{n} \sum_{i=1}^n |y_i - \hat{f}_K(x_i)|^q$$

where q is set to 2 to provide the conditional expectation of the mean, $p = 1 + (K-1)(d+2)$, and d is the number of predictor variables. The minimization quantity is a generalization of the least squares minimization criteria, with the addition of a penalty for increasing number of basis functions K through the $\left(\frac{n}{n-p} \right)^q$ term. Full details of the stochastic approximation algorithm used to minimize $R_{GCv}(\hat{f}_K)$ are given in Hooper [2001].

A threshold was determined under the ALB model in the same way as the simple sigmoidal model, by obtaining the maximum values of $f''(x)$. This was similar to Hooper's [2001] examination of the first derivative to determine a threshold value between aerobic and anaerobic metabolism. Because the ALB model can yield more

complicated gradients, special care was taken to ensure that maxima of $f''(x)$ were not inappropriate local values.

3.2.2.4. Interval-based threshold estimation

To complement the regression-based methods, a simple technique was borrowed from the environmental health literature. The studies of Davis et al. [2003a,b] analyzed the relationship between heat waves and elevated mortality in several US cities, finding that above a certain threshold of outside air temperature, the number of deaths in a given area increases rapidly. For their analysis of daily air temperature and mortality in Chicago during the 1960's and 1970's, for example, it was found that above 30°C, the number of deaths increases rapidly (Davis et al. [2003a], their Figure 1). To identify the threshold value, the daily mortality values were aggregated into 2°C class intervals, with the mean mortality calculated for each interval, and then compared to the overall mean using a one-tailed t -test. The threshold temperature was defined as that for which the mortality remained significantly above average for all higher temperature intervals at the 5% significance level.

Application of this technique to the drought-haze analysis was straightforward. For each moisture index, mean $\ln(B_{ext})$ values were calculated across hourly observations pooled from all stations in the analysis domain, for 50 moisture intervals, with the interval width varying according to the scale of the moisture index. When the $\ln(B_{ext})$ remained significantly above average below a certain moisture level, this moisture level was defined as the threshold. To account for potentially non-normal distributions of $\ln(B_{ext})$ within each interval, empirical 95% bootstrap confidence intervals were also calculated.

3.2.2.5. Model evaluation

The models and predictors were compared according to their goodness of fit, degree to which their parameter and threshold estimates were well constrained, and their overall complexity. In the case of the change point and sigmoidal models, the number of unsuccessful bootstrapped model fits was also considered, with models having higher fit rates preferred over those with low fit rates.

The adjusted coefficient of determination (R^2) was used to compare the fitted models, and is given by

$$R^2 = 1 - \left(\frac{n-1}{n-p} \right) \left(\frac{SSE}{SSTO} \right)$$

where n is the number of observations, p is the number of model parameters. SSE is the error sum of squares $SSE = \sum_{i=1}^N (\hat{y}_i - y_i)^2$ and $SSTO$ is the total sum of squares

$$SSTO = \sum_{i=1}^N (y_i - \bar{y})^2, \text{ where } \hat{y}_i \text{ are the predicted } \ln(B_{ext}) \text{ values, } y_i \text{ are the observed}$$

$\ln(B_{ext})$ values and \bar{y} is the mean of the observed $\ln(B_{ext})$ values. The R^2 statistic measures the proportion of total variation in the predicted variable explained by the model, and the $\frac{n-1}{n-p}$ term allows for comparison between models with different degrees of freedom.

The model assessment was naturally directed towards periods of severe drought and haze, and so R^2 was examined for across four different intervals of the data set: the whole range, and the bottom 50%, 25%, 10% of the moisture data. Looking specifically at R^2 over the bottom 10% of the moisture data for example allowed evaluation of the models' ability to model the full magnitude of severe haze, and guarded against R^2 values being dominated by the model fit over normal, non-haze periods, which form the majority of cases.

Because of the operational potential of the analysis, specific attention was given to outliers in situations where the drought index failed to capture a severe haze period. The consistency of different indices and models across the two analysis domains was also considered. That is, if a model or index performed consistently well in both of Sumatra and Kalimantan, it was preferred over a model that might have performed slightly better in one domain, but significantly poorer in the other. Of note though, is that threshold estimates need not agree between Sumatra and Kalimantan; owing to different land-use pressures and landscape disturbance, the sensitivity of the two

regions to drought may be different. The relative complexity of moisture indices and computational requirements was also considered, with simpler indices preferred.

Another obvious way of estimating a drought threshold would have calibration using a well-fitted regression model. For an extinction coefficient defined as hazardous, the corresponding moisture level could be estimated using inverse prediction from the fitted curve. Unfortunately, no objective definition of a hazardous extinction coefficient was available for Indonesia, or any regions in Southeast Asia. The only available guidelines found were from the Montana Department of Environmental Quality prescribed burning program (see <http://www.deq.state.mt.us/FireUpdates/Breakpoints.asp>), which included visibility levels (and hence extinction coefficient) in its classification of air quality guidelines. The difference in fire environments and ambient air quality levels was presumed too great for the Montana guidelines to be applied in an Indonesian context.

4. Results and Discussion

4.1. Meta-data characteristics

The dataset acquired from the NCDC contained 5 876 998 records across 176 stations in Indonesia, with the availability of data varying significantly from year to year. There were two main periods of data availability: from 1942 to 1965 and from 1973 to 2003. The availability of data prior to the founding of the WMO in 1950 is surprising, given that the shared distribution and archiving of synoptic weather data was prompted by the WMO's founding. Even though limited, the availability of data from 1942 to 1945 is especially notable, as this was the period of Japanese occupation in Indonesia, during which contact and data occupation with Western institutions would have been limited. Data availability generally increased from 1950 through 1965, with a complete absence of data from 1966 to 1972. Initially, the drop off in data in 1965 could be attributed to the start of Indonesia's period of political instability, but examination of records from Malaysia and Singapore also showed an absence of data over the same period. It is likely therefore, that data in fact exists, but was not archived at the NCDC, although the reasons for this absence are unclear.

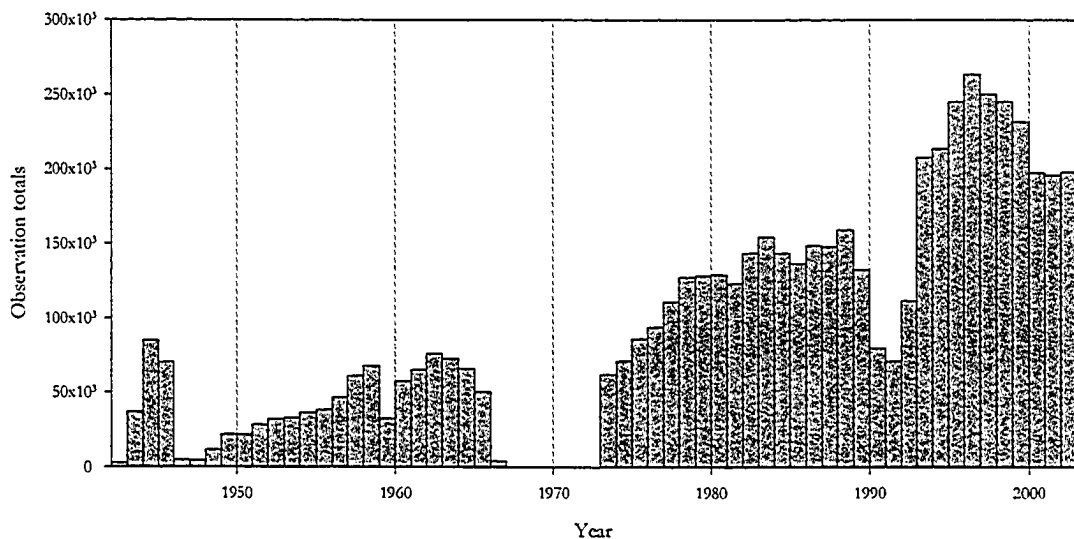


Figure 7. Total number of observations per year across all Indonesian stations

The availability of these records offers a significant new source of raw synoptic data in a digital format. In their meta-analysis of data availability in Southeast Asia, Page et al. [2004] found that Indonesian synoptic data dating back to 1950 was only

available in hardcopy format, when in fact the analysis here has shown that a substantial amount of digitized data are available. This is highly significant in light of current data recovery efforts at the Indonesian Bureau of Meteorology and Geophysics, in that data recovery and digitization should be focused on the 1966-1972 period, for which the NCDC has no data. Given the cost and effort in recovering hardcopy records, intensive digitization for other periods would risk a significant waste of resources.

Over the two analysis regions, data availability reached a minimum from 1990 through 1992 (Figure 8). In Sumatra, data availability before and after this period was comparable, with weak data periods in the first half of 1981 and early 2000. In Kalimantan, data availability surged after 1993, due largely to the apparent addition of several standard reporting hours (not shown).

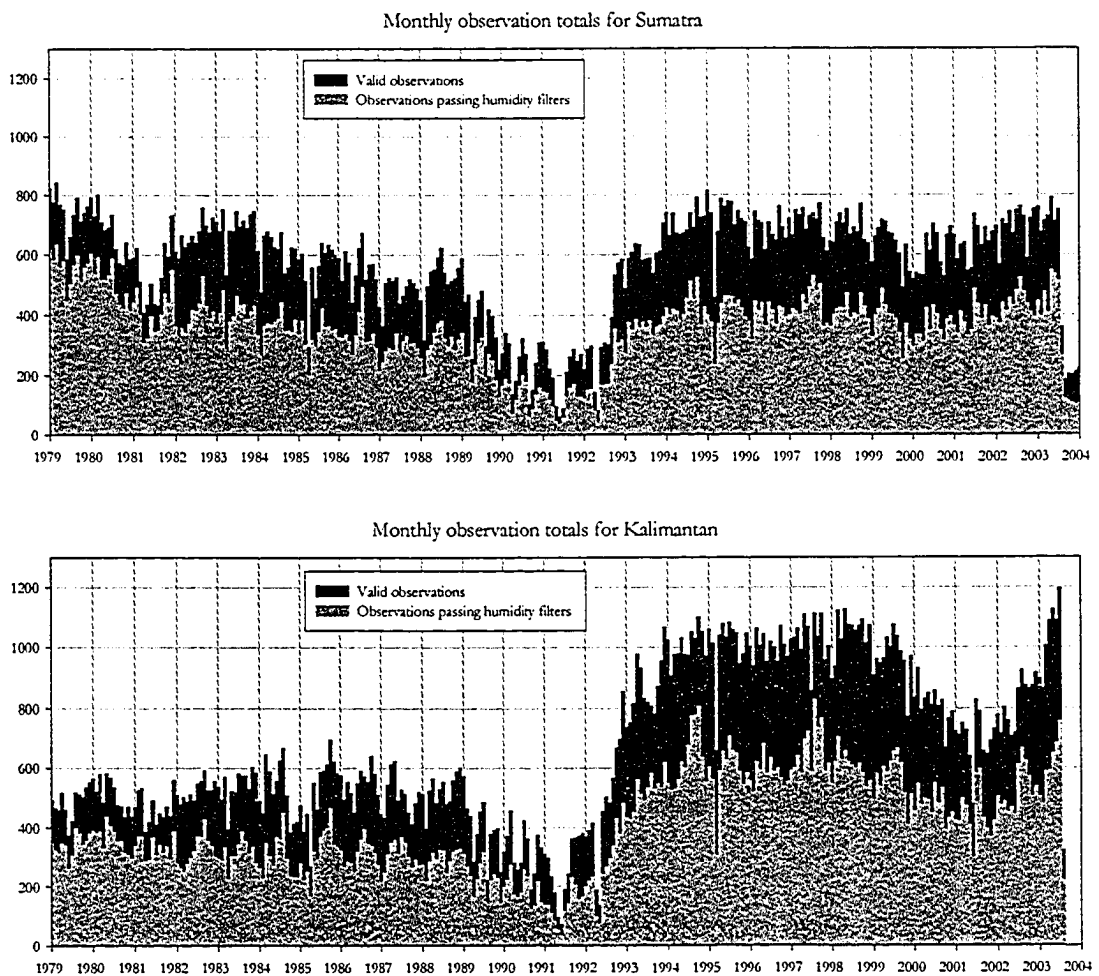


Figure 8. Monthly observation totals for Sumatra (top) and Kalimantan (bottom)

4.2. Qualitative analysis of haze and moisture signals

The haze and moisture signals for Sumatra and Kalimantan are shown in Figure 9 and Figure 10 respectively, with the severe haze events for both regions summarized in Table 2. In both Sumatra and Kalimantan the episodic nature of the haze episodes is apparent from the time series data. Despite regular periods of reduced rainfall in normal year dry seasons, it is only when rainfall drops below a given threshold that the severe haze occurs. Due to the direct effects of the ENSO cycle on Indonesian rainfall, this is in distinct contrast to the significant biomass burning Amazonia, which occurs on a regular annual cycle [Herman et al., 1997, their Figure 7].

Although both estimate the same physical phenomenon, the area-averaged PRECL and GPCP signals showed differences. Over Sumatra, the three month total PRECL values were on average 10% higher than the GPCP estimates, whereas in Kalimantan PRECL estimates were on average 5% less than the GPCP estimates.

Sumatra haze events

In Sumatra, the most significant haze episodes were during the dry seasons of 1982, 1991, 1994 and 1997 with smaller episodes in 1987 and 2002, as shown by Wang et al. [2004]. The episode in 1982 started in August, reached a peak $\ln(B_{ext})$ value of -0.170 in September, and ended in November. The 1987 event was less severe, starting in September and lasting only until October, reaching a smaller peak value of -0.880. The haze events of the 1990's in Sumatra increased substantially in magnitude. The 1994 event was comparable in onset and duration to 1982, but reached a much higher peak of 0.937. Similarly, the 1994 event lasted from August through November, but reached near equal peak values of 0.414 in September and 0.447 in October. The 1997 event was the most severe. Like 1994, there was a 2-month long peak, but at much higher values of 1.036 in September and 1.256 in October, and ending in November. This October peak is in agreement with the regional TOMS analysis of Nakajima et al. [1999], which also showed an October peak. The 2002 episode was notably less severe, lasting only during September and October, during which it reached a peak value of -0.958.

Kalimantan haze events

In Kalimantan, there were strong episodes during the dry seasons of 1982, 1987, 1991, 1994, 1997, 2002 and perhaps the neutral ENSO year of 2001. There are also two wet-season episodes in early 1983 and 1998, corresponding to medium-range transport of haze from East Kalimantan, which will be discussed in the context of the regression model results in the next section. The event in 1982 lasted through September and October, reaching near-equal peak values of -0.948 and -0.824. The 1987 event was also quite moderate and had the same duration with a peak value of -0.989 in September. The 1991 event occurred from September through November, with an October peak of -0.498. The 1994 event was similar in duration to 1991, but had multiple September and October peaks of -0.593 and -0.628, respectively. The 1997 was unprecedented for Kalimantan. It started in August, a month earlier than any previous event, and stayed at values higher than any previously observed until October, with a September peak of 1.257, and termination in November. There was a small, but distinct event during August of 2001 with a peak value of -1.096. In 2002, a strong episode occurred from August until October with a September peak value of -0.7645.

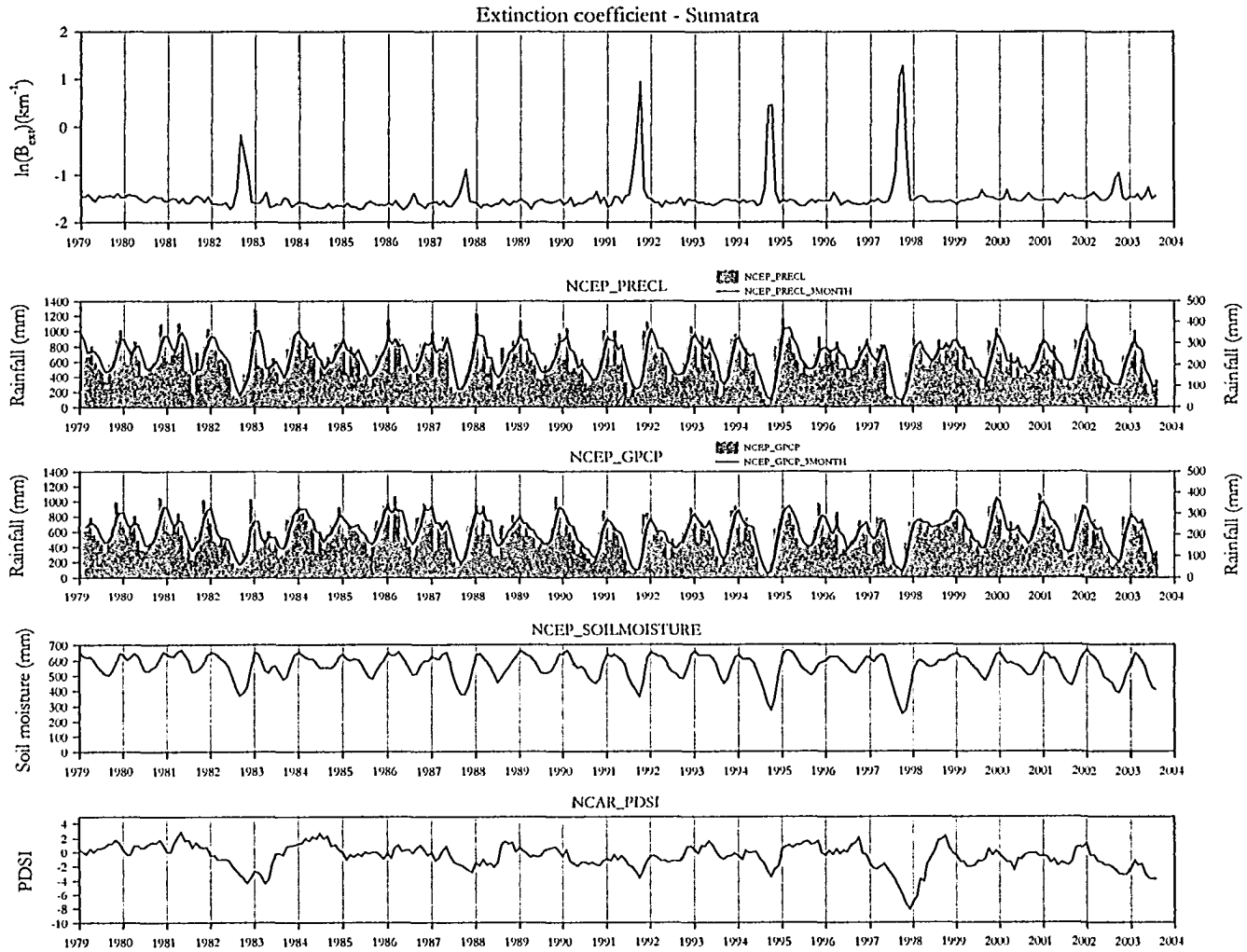


Figure 9. Extinction coefficient and moisture signals for Sumatra. In the GPCP and PRECL series, grey bars show the monthly rainfall total and the black solid line shows the 3-month running total.

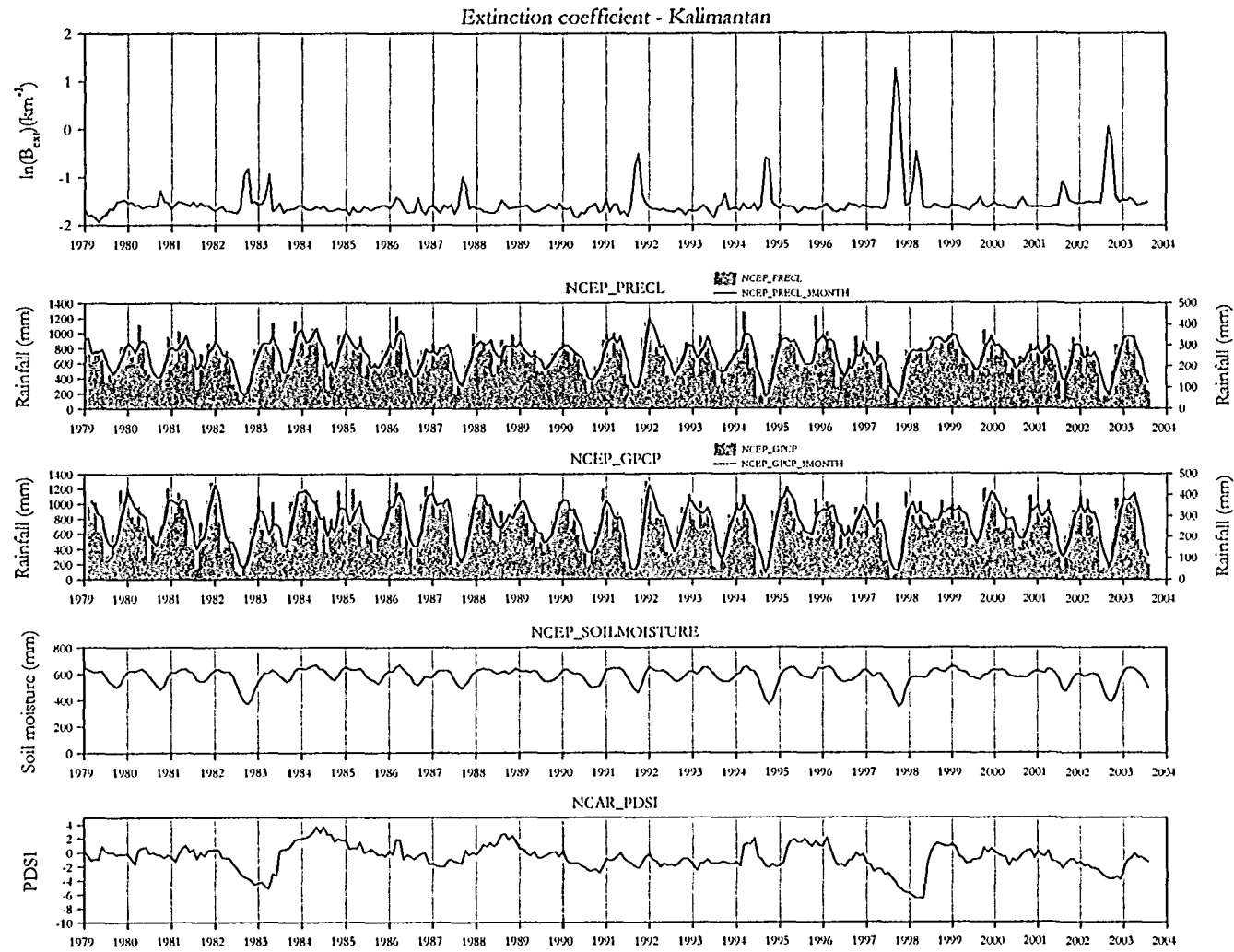


Figure 10. Extinction coefficient and moisture signals for Kalimantan. In the GPCP and PRECL series, grey bars show the monthly rainfall total and the black solid line shows the 3-month running total.

Year	Sumatra			Kalimantan		
	Start	End	Maximum	Start	End	Maximum
1982	August	November	September peak of -0.170	September	October	September peak of -0.948 October peak of -0.824
1983				April	April	April peak of -0.934
1987	September	October	October peak of -0.880	September	October	September peak of -0.989
1991	August	November	August peak of 0.937	September	November	October peak of -0.498
1994	August	November	September peak of 0.414 October peak of 0.447	September	October	September peak of -0.593 October peak of -0.628
1997	July	November	September peak of 1.036 October peak of 1.256	August	November	September peak of 1.257
1998				February	April	March peak of -0.467
2001				August	September	August peak of -1.096
2002	September	October	October peak of -0.958	August	October	September peak of .047 October peak of -0.207

Table 2. Timing and severity of major haze events in Sumatra and Kalimantan indicated from regional $\ln(B_{ext})$ signals.

Underlying moisture conditions

Over both domains, the PRECL, GPCP, and SOILM signals each show a strong correspondence, with a regular wet and dry seasons, and anomalously low rainfall during the warm ENSO years of 1982, 1987, 1991, 1994 and 1997, and perhaps 2002. The PDSI signal clearly shows the droughts only in 1982/83 and 1997/98, with smaller anomalies in 1991 and 1994 in Sumatra. As a relative signal the character of the PDSI droughts is substantially different than the other three, amplifying the large events, with the smaller events less evident. During early 1983 and 1998, for example, low PDSI values remain through periods of substantial precipitation, as indicated by the two precipitation series. The effect of antecedent moisture in the PDSI would therefore appear to be quite strong, as was the case in Quiring and Papakryiakou's [2003] analysis of PDSI performance as an agricultural drought indicator in Canada.

Nichol [1998] and Hendon [2003] suggested that transmigration and consequent land use change have increased the sensitivity of the fire-climate system in Indonesia. Both note that although 1982 was much stronger in terms of both ENSO strength and drought in Indonesia, the accompanying haze was much weaker than in 1994 or 1997, but no supporting data are provided. Siegert et al. [2001] suggested an increase in landscape flammability due to increased logging and forest activity. The possible effects of transmigration and land use change in both regions can be determined by looking anecdotally at individual events, and how the magnitudes of haze events might have changed over time with respect to the strength of drought.

In Sumatra, the effects of land use change can be seen most clearly by comparing the months of September for the 1991, 1994 and 1997 events (Figure 11), in this case using 3-month GPCP rainfall as the moisture index. In September 1991 a 3-month rainfall total of 86mm yielded an $\ln(B_{ext})$ of -0.20, and in September 1994 a 3-month rainfall total of 40mm yielded an expectedly larger $\ln(B_{ext})$ of 0.41. In September of 1997, drought conditions were less severe, with a 3-month rainfall total of 108. The haze conditions though were substantially more severe than in 1991 or 1994, with $\ln(B_{ext})$ of 1.03, which aside from the peak obtained in the following month, was the

highest $\ln(B_{ext})$ value on record. Between the 1991/1994 and 1997 events then, it would appear that the fire environment in Sumatra became increasingly sensitive to drought. It is difficult to discern any land-use effect prior to the 1990's, as the drought events in Sumatra for 1982 and 1987 were much less severe than in the 1990's.

The same phenomenon would appear to hold for Kalimantan as well. The 3-month rainfall totals for September during 1991 and 1997 were comparable at 121mm and 123mm respectively, but the haze in 1991 had a $\ln(B_{ext})$ of only -0.80 compared to 1.26 in 1997, the most severe value seen on record for Kalimantan (Figure 12). Unlike in Sumatra, a similar pattern can be seen in Kalimantan over the long-term by comparing the haze events of 1982 and 2002. In September of 1982, a 3-month total rainfall of 149mm yielded a moderate $\ln(B_{ext})$ of -0.95, whereas in September of 2002, a higher rainfall value of 164mm yielded a much more severe $\ln(B_{ext})$ of 0.05.

October of 2002 in Kalimantan presents a disturbing case. The haze achieved a $\ln(B_{ext})$ of -0.21, which is not particularly severe, except that it occurred at a rainfall level of 288mm, compared to 1991 and 1994, whose lower October $\ln(B_{ext})$ values of -0.50 and -0.63 occurred under much lower rainfall levels of 208mm and 190mm respectively. In Kalimantan therefore, there is reason to believe that the potential for severe haze has continued to increase dramatically, and that a future drought on the order of 1997, or even 1994, will yield an unprecedented amount of haze.

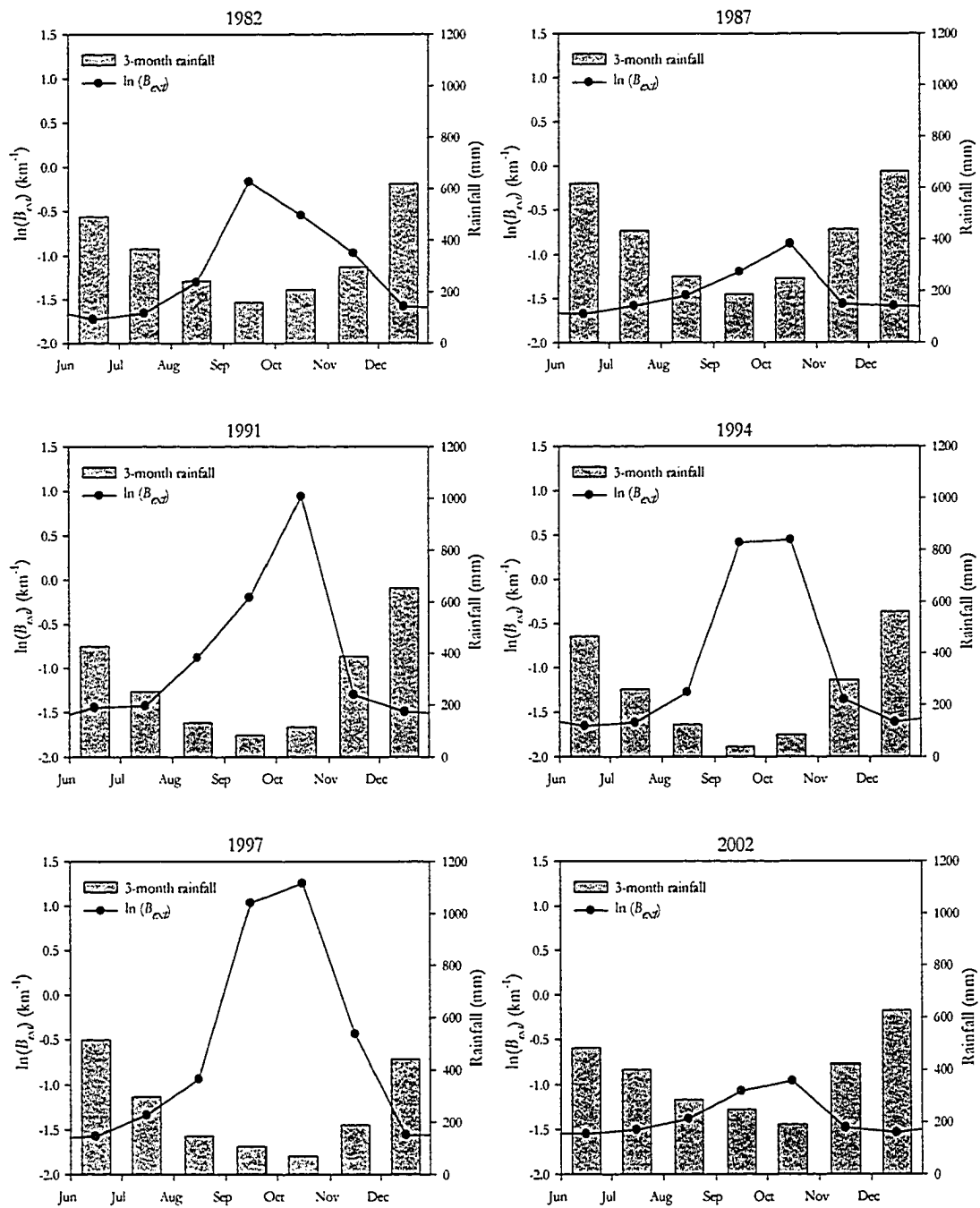


Figure 11. GPCP rainfall and extinction coefficient for severe haze events, Sumatra

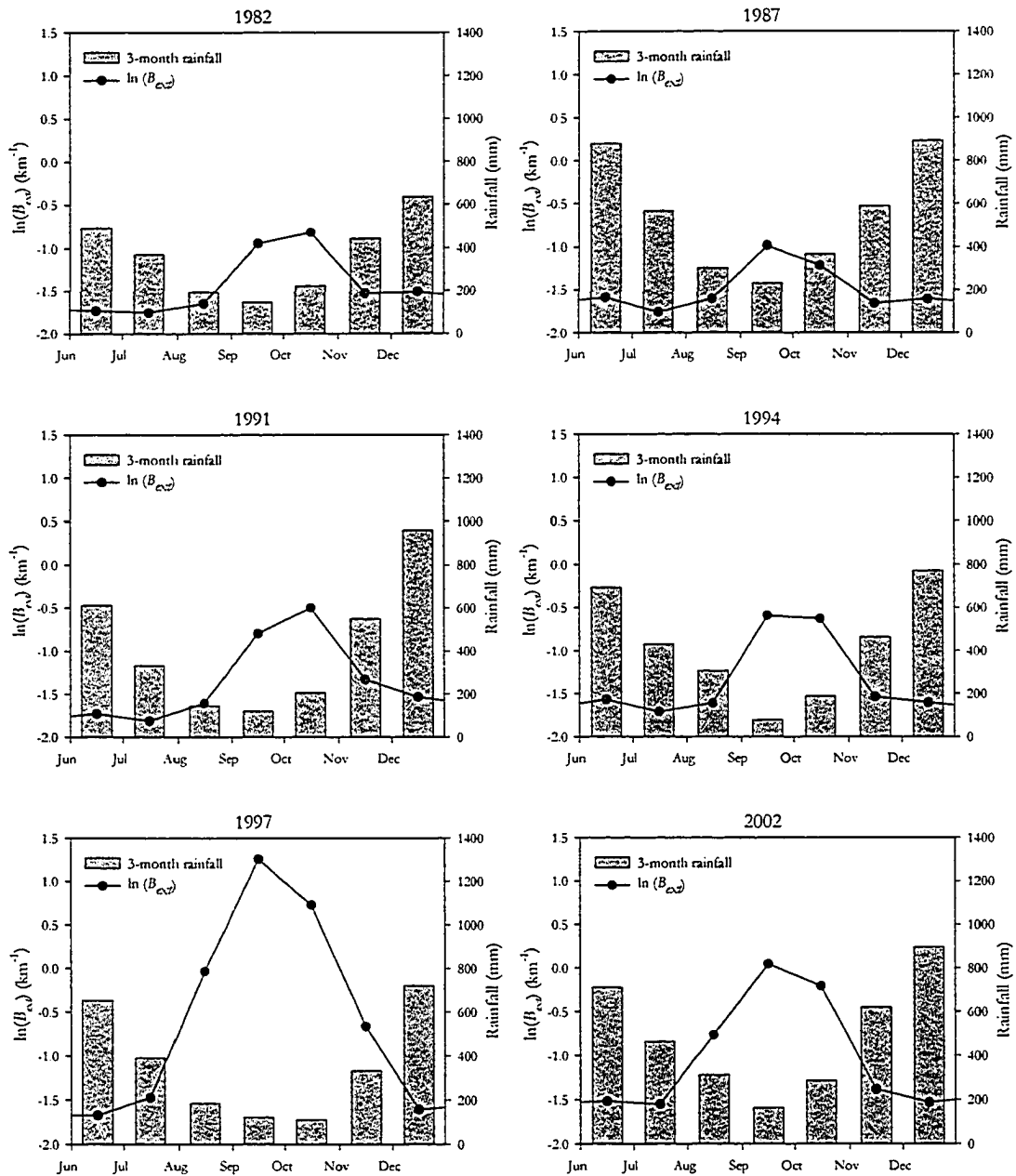


Figure 12. GPCP rainfall and extinction coefficient for severe haze events, Kalimantan

4.3. Regression results

There was a strong nonlinear relationship between moisture and haze over the analysis period. In both Sumatra and Kalimantan, the GPCP 3-month rainfall, PRECL 3-month rainfall, and SOILM soil moisture model were the best predictors of haze, with the PDSI performing poorly. Fitted models are shown for Sumatra in Figure 13

and for Kalimantan in Figure 14. The adjusted coefficient of determination R^2 for different data intervals is shown in Table 3, and parameter estimates and residuals for all models are provided in Appendix A.

Sumatra

For each of the PRECL, GPCP and SOILM indices, apparent thresholds appear at 350mm, 250mm and 450mm, respectively; the detailed threshold estimates will be described in the next section. Above these thresholds there is regularly variability about a normal $\ln(B_{ext})$ value of roughly -1.5. Below the threshold values variability of $\ln(B_{ext})$ tends to increase, confirming the need to assess model quality over different intervals of the moisture indices. Visually, all models appear well fit over the transition region of the PRECL, GPCP and SOIL indices.

In Sumatra, the best models were the change point and ALB models using GPCP as a predictor, which both had an overall R^2 of 0.78 and a 10% R^2 of 0.68. The PRECL and SOILM models had slightly lower, but still reasonable R^2 values for the ALB and change point models. The ALB estimate with PRECL as the predictor had more basis functions ($K=5$) than for the GPCP or SOILM predictors, and consequently improved the fit over the below threshold values compared to the change-point model ($R^2 = 0.64$ for ALB, $R^2 = 0.59$ for change point).

In general, the sigmoid model is less applicable, because of not fully capturing the full magnitude of severe haze events, prematurely flattening out at 0 due to the limited vertical scaling of model. This is reflected by the sharper drop in R^2 values over smaller data ranges. In contrast, the predicted $\ln(B_{ext})$ values under the change point and ALB models continue to increase with decreasing moisture for each of the PRECL, GPCP and SOILM models. The GPCP and SOILM indices show particularly strong agreement over the increasing part of the curve, with a greater variation in model with the PRECL index. The β_1 slope obtained in change point model also appears to be a good approximation to that of the curves for GPCP and SOILM, and to the sigmoidal curve of the PRECL. There were no serious outliers in Sumatra in terms of missed haze events for the PRECL, GPCP or SOILM predictors.

In Sumatra, the PDSI performs poorly under all models. Although there is an apparent threshold for the PDSI around -2.0, there is substantially more variability over below threshold $\ln(B_{ext})$ values than with the other moisture indices, as is indicated by the much lower R^2 values. The ALB model is over fit using the PDSI, using $K=10$ basis functions and yielding a physically implausible model for below threshold values. This is due to the strong effect of the cluster of three outliers at the $\ln(B_{ext}) = -1.5$ level with PDSI values of less than -6.0. Neither of the change point or sigmoid models are well fit for below threshold values, again due to the cluster of values below a PDSI of -6.0. These outliers occur during the three-month period from December 1997 through February 1998, during which no haze was present in Sumatra. Whereas the other three indices captured the moisture recovery brought on by the wet season rainfall, the PDSI continued to remain at significantly below normal values (Figure 9). The superiority of the PRECL, GPCP and SOILM indices is also reflected by the convergence rates for the change-point bootstrap estimates, with 96.8% of PRECL, 95.8% of GPCP and 96.3 of fit attempts converging, compared to only 66.3% for the PDSI.

Kalimantan

For each of the PRECL, GPCP and SOILM indices, apparent thresholds appear at 400mm, 300mm and 500mm respectively, slightly higher than in Sumatra. As with Sumatra, the variability of the $\ln(B_{ext})$ increases below these threshold values.

In Kalimantan, the models had weaker performance compared to Sumatra. The PRECL index proved to be the best predictor, with similar 100% R^2 values of .60 and 10% R^2 values of 0.52 across all three models. There was also good R^2 agreement across models for the GPCP and SOILM predictors, though values were overall much lower than the PRECL. The more similar R^2 values can be seen from the closer agreement in model shape for each of the three indices. Unlike in Sumatra where only the sigmoidal model under-predicted the full magnitude of the severe haze event, none of the models captured the full magnitude of the severe haze event. As in Sumatra, the PDSI performed poorly, with low R^2 values across all models. In

agreement with the lower R^2 values, the convergence rates for the bootstrapped change-point estimate were lower in Kalimantan than in Sumatra (Table 6).

Serious outliers also appeared in Kalimantan for the PRECL, PGPC and SOILM models, where significant haze occurred at far higher than expected levels of moisture. For the PRECL models, this appears as the cluster of four observations between the 800mm and 900mm levels. One of these observations occurred in April of 1983, and the other three were over the period from February to April of 1998. In an operational setting, this would represent a serious failure of any drought monitoring system, and so warrants specific attention.

The haze experienced over the southern Kalimantan analysis domain can be explained by long-distance smoke transport from fires in East Kalimantan. During each of these periods, significant burning was occurring in East Kalimantan under conditions of highly localized drought [Goldammer and Seibert, 1990; Siegert and Hoffman, 2000]. To confirm that East Kalimantan was a potential source of the haze, monthly mean wind vectors at the 850mb level were plotted from the Reanalysis data [Kalnay et al., 1996], using the online plotting system available at the University of Oklahoma (see <http://weather.ou.edu/~cgodfrey/reanalysis/>), shown in Figure 15 and Figure 16. During both events, wind flow into southern Kalimantan is from the northeast, directly from East Kalimantan, confirming that burning significant burning in East Kalimantan was a likely source of unexpected haze in Southern Kalimantan. Examination of individual station data (not shown) also shows that haze was much stronger in the eastern-most analysis station (965950) than in stations further away from East Kalimantan.

Across Sumatra and Kalimantan then, the ALB and change-point models using simple rainfall-based indices performed best. The sigmoidal curve captures the transition from above to below threshold values well, but in Sumatra failed to capture the magnitude of the haze events. The GPCP was best in Sumatra, and the PRECL best in Kalimantan, though it is important to observe that with its increased flexibility the ALB-PRECL model approached the quality of the ALB-GPCP model in Sumatra. It would appear then that the more complicated soil-moisture models offered no

advantage over the simple rainfall-based indices, and in the case of the PDSI, have little predictive power.

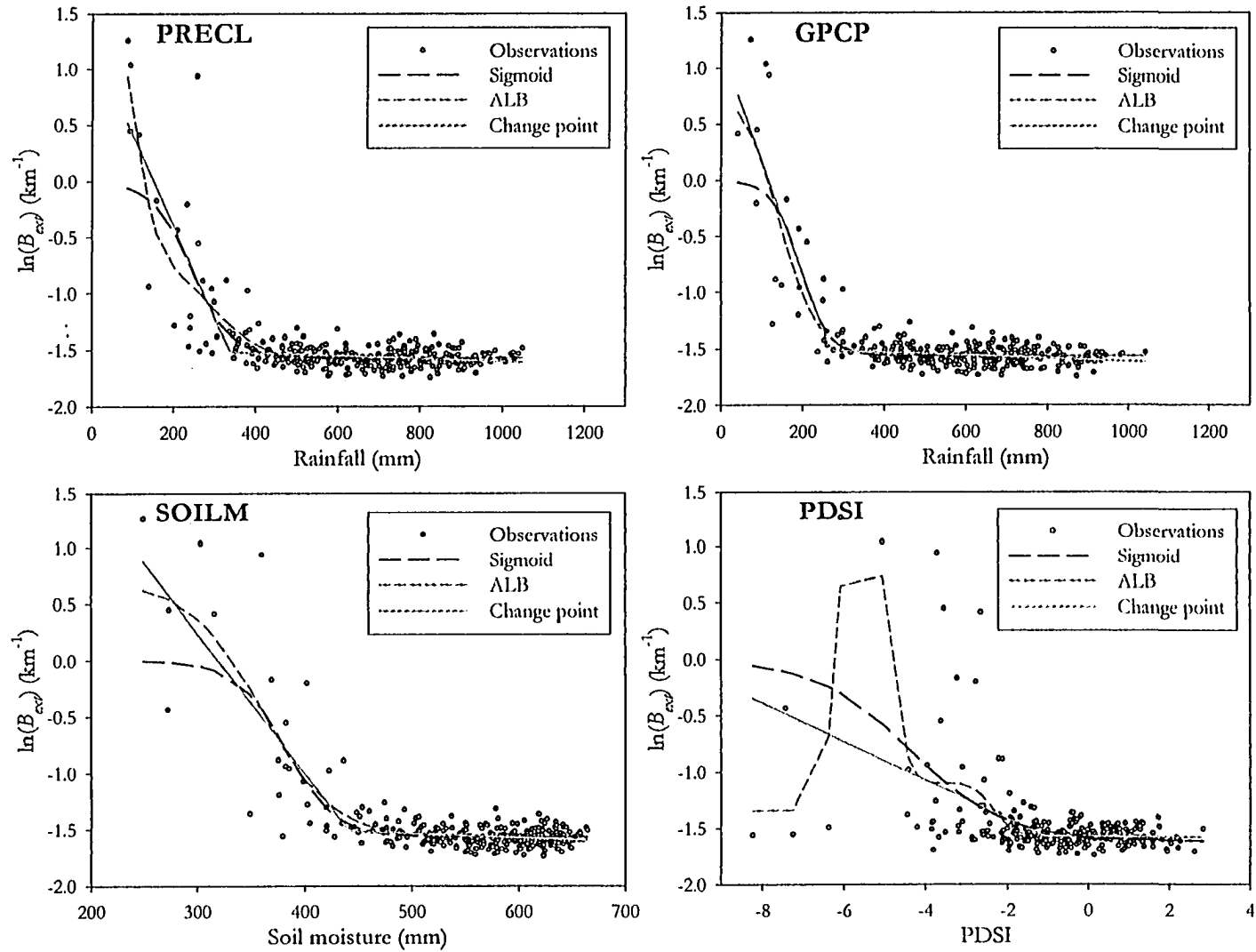


Figure 13. Fitted regression models for Sumatra

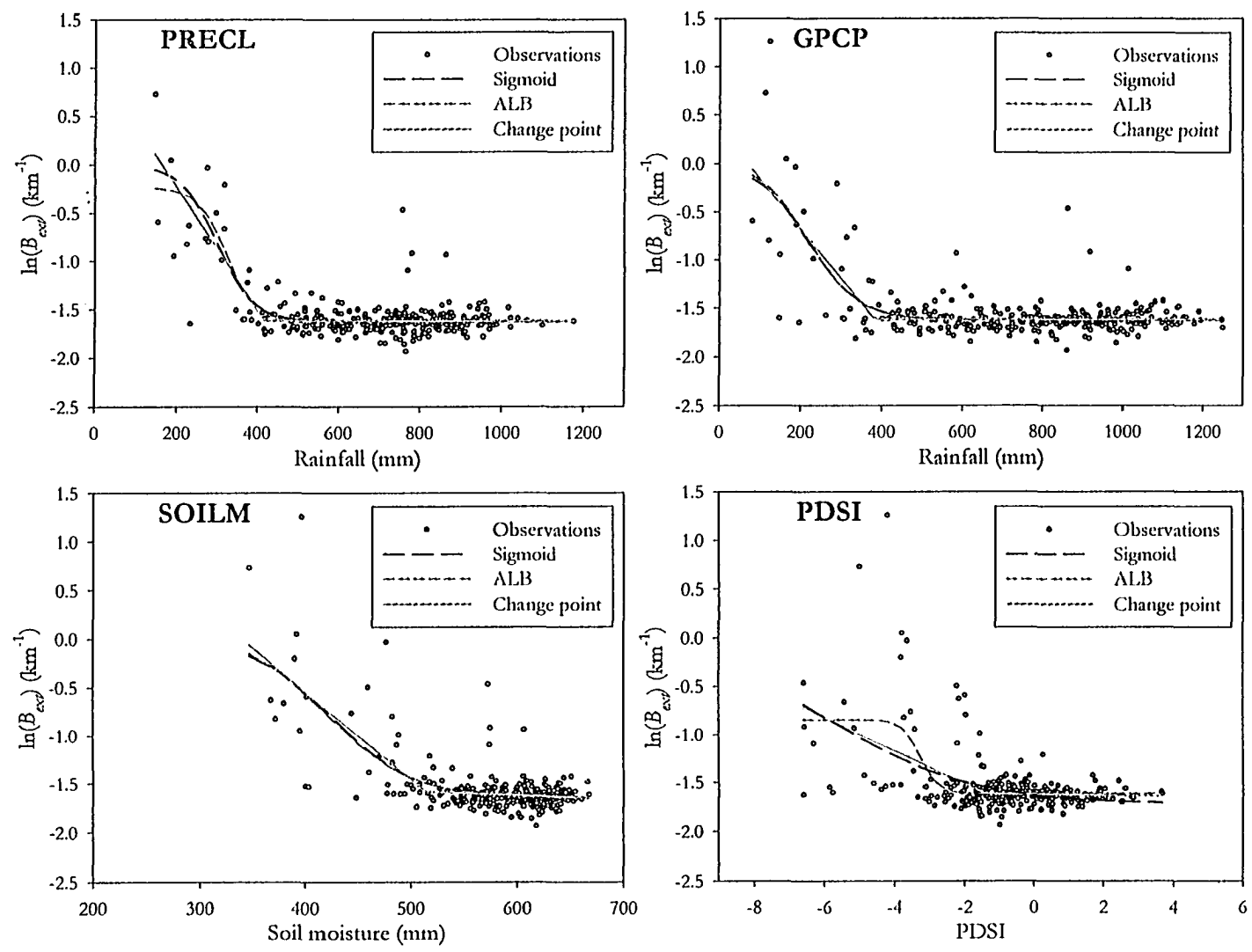


Figure 14. Fitted regression models for Kalimantan

Sumatra												
Quantile	Change point				Sigmoidal				ALB			
	100	50	25	10	100	50	25	10	100	50	25	10
PRECL	0.7190	0.7194	0.6911	0.5861	0.6720	0.6676	0.6295	0.4951	0.7490	0.7529	0.7289	0.6395
GPCP	0.7797	0.7844	0.7707	0.6816	0.7409	0.7422	0.7202	0.6100	0.7815	0.7864	0.7718	0.6847
SOILM	0.7436	0.7461	0.7232	0.6166	0.7116	0.7109	0.6817	0.5563	0.7487	0.7520	0.7291	0.6237
PDSI	0.2462	0.2119	0.1154	-0.0103	0.2325	0.1988	0.1036	-0.0069	0.4377	0.4218	0.3554	0.3109

Kalimantan												
Quantile	Change point				Sigmoidal				ALB			
	100	50	25	10	100	50	25	10	100	50	25	10
PRECL	0.6030	0.6677	0.6414	0.5237	0.6011	0.6658	0.6382	0.5170	0.6016	0.6686	0.6414	0.5228
GPCP	0.5362	0.5764	0.5560	0.3949	0.5376	0.5777	0.5571	0.3964	0.5313	0.5720	0.5511	0.3881
SOILM	0.5426	0.5414	0.5494	0.3663	0.5350	0.5325	0.5383	0.3511	0.5294	0.5267	0.5329	0.3441
PDSI	0.2536	0.2252	0.1543	-0.0103	0.2263	0.1991	0.1329	-0.0069	0.3147	0.2916	0.2328	0.1110

Table 3. Adjusted coefficient of determination (R^2) for different predictors and regression models, for different intervals of the moisture indicators

850 mb monthly mean winds at 00Z for APR 1983

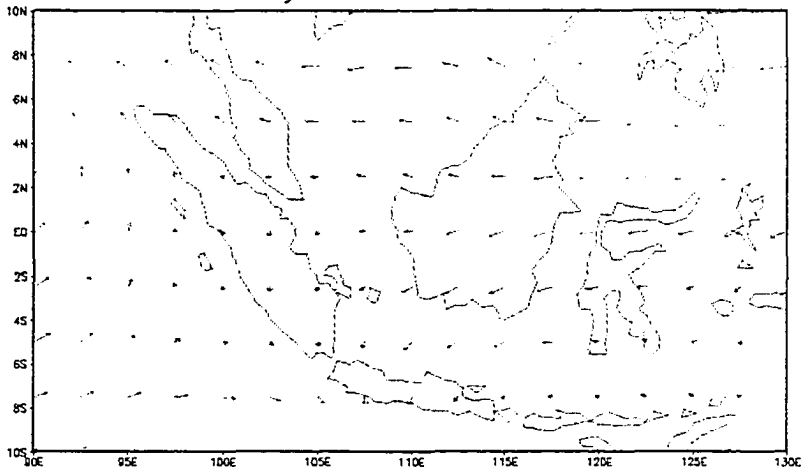
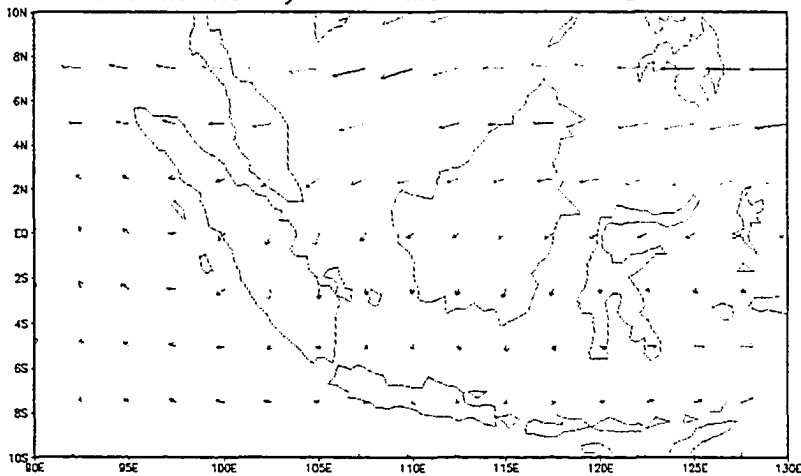
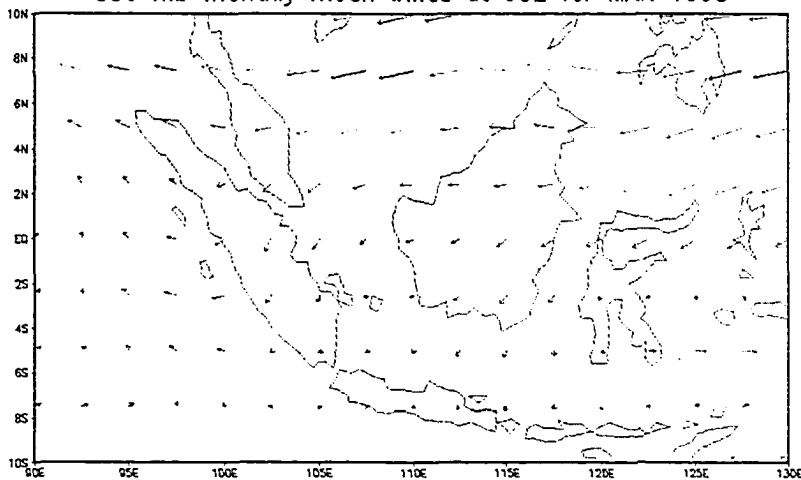


Figure 15. 850 mb monthly mean winds from the NCAR Reanalysis, April 1983

850 mb monthly mean winds at 00Z for FEB 1998



850 mb monthly mean winds at 00Z for MAR 1998



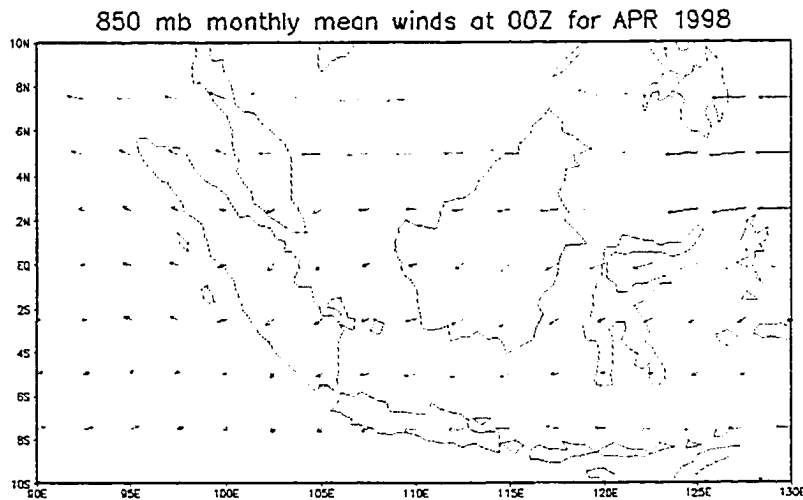


Figure 16. 850 mb monthly mean winds from the NCAR Reanalysis, February 1998 (top), March 1998 (middle) and April 1998 (bottom)

4.4. Moisture thresholds

The moisture threshold estimates under each model and predictor are summarized in and plotted in Figure 19. The results for the interval-based threshold estimation are shown for Sumatra in Figure 17 and for Kalimantan in Figure 18. The regression results indicate that there is no advantage to using the more sophisticated SOILM and PDSI indices, and so the discussion is focused on the PRECL and GPCP rainfall-based indices.

In Sumatra, the PRECL threshold estimate under the change-point was 337.26mm with a 95% confidence interval of (247.83mm, 404.93mm). The threshold estimate was slightly lower under the sigmoidal model at 301.99mm with a narrower 95% confidence interval of (241.57mm, 339.70mm). The ALB threshold was 382.48mm and the interval-based threshold was 346.44mm, both within the range spanned by the confidence intervals of the change-point and sigmoidal models. The GPCP threshold estimates were 273.97mm (211.899 mm, 316.73 mm) for the change-point model and 237.71mm (192.69mm, 263.19mm) for the sigmoidal model, both slightly lower than their corresponding PRECL thresholds, which in part reflects the GPCP bias towards lower rainfall values in Sumatra. As with the PRECL index, the ALB threshold of 204.58mm and interval-based threshold of 290.29mm were within the range spanned

by the confidence intervals of the change-point and sigmoidal models. The SOILM threshold estimates cannot be directly compared to the rainfall-based indices, but also showed good agreement across models.

In Kalimantan, the threshold estimates were higher than in Sumatra. The PRECL estimate was 414.25mm (381.01mm, 467.89mm) for the change point model and 351.20mm (321.82mm, 375.03mm) under the sigmoidal model. Using the GPCP index, the change point threshold was 378.65mm (272.40mm, 455.81mm), and the sigmoidal threshold was 294.71mm (225.95mm, 341.29mm). Like in Sumatra, the ALB and interval-based estimates fell within the combined 95% intervals of the change-point and sigmoidal threshold estimates for the PRECL and GPCP indices. On the whole then, Kalimantan would therefore appear more sensitive to drought conditions than Sumatra. Also, there was less overall difference between the PRECL and GPCP thresholds for Kalimantan, due to the smaller bias between the two rainfall signals than in Sumatra. The SOILM threshold estimates showed general agreement, although the confidence interval under the changepoint model was notably wide.

As might have been expected from the regression results, the PDSI threshold estimates were problematic over both domains, and lacked the consistency between models of the other indices. The sigmoidal model estimate in Sumatra, for instance, had an upper 95% confidence interval greater than the maximum observed PDSI value. The interval-based thresholds were also unreasonably low, owing to the wide range of $\ln(B_{ext})$ values seen at low PDSI values.

Looking at the overall results across indices and both regions, the behavior of the models can be determined. The importance of the non-parametric bootstrap technique in estimating threshold confidence intervals was also shown, as the confidence intervals were asymmetric in most cases (Figure 19). Of the three regression methods, the sigmoid and ALB models consistently gave lower estimates than the change-point regression methods in all but one case. The ALB estimate for Sumatra under the PRECL model was an exception, due to the greater number of basis functions in the ALB estimate, and consequent more complicated function. The threshold estimates were therefore sensitive to the estimation technique.

There is the possibility that the gradient-based threshold definitions give estimates too low to be useful operationally. Looking at the example sigmoidal curve in Figure 6, for example, another possible threshold region appears between $x = 250$ and $x = 300$, where the curve begins to exhibit distinct curvature. This would correspond to the local maximum of $f''(x)$ which occurs at $x = 270$, although the physical interpretation of higher derivatives becomes more difficult.

In contrast, no such difficulty exists with the change point model, as the meaning of the α parameter corresponds unambiguously to the threshold value. Although the change-point model is not as physically realistic in modeling the transition from non-drought to drought conditions, it is perhaps the preferable estimation technique, and was therefore selected to define operational threshold values.

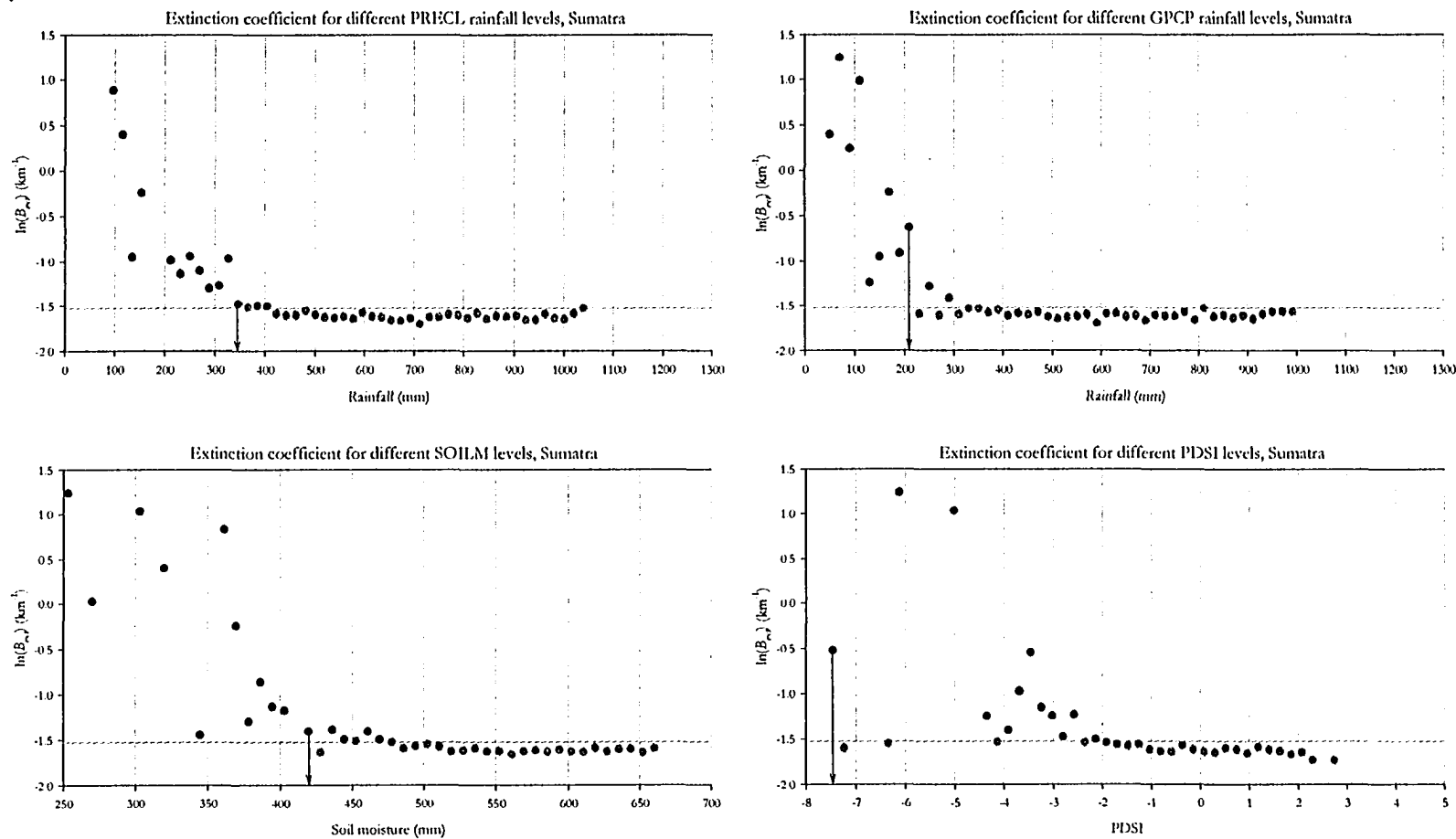


Figure 17. Interval-based thresholds for Sumatra, PRECL (top left), GPCP (top right), SOILM (bottom left) and PDSI (bottom right). Black circles indicate class intervals significantly above the baseline value, grey circles indicate class intervals not significantly above the baseline, the grey horizontal line indicates the baseline value, and the black arrow indicates the threshold value.

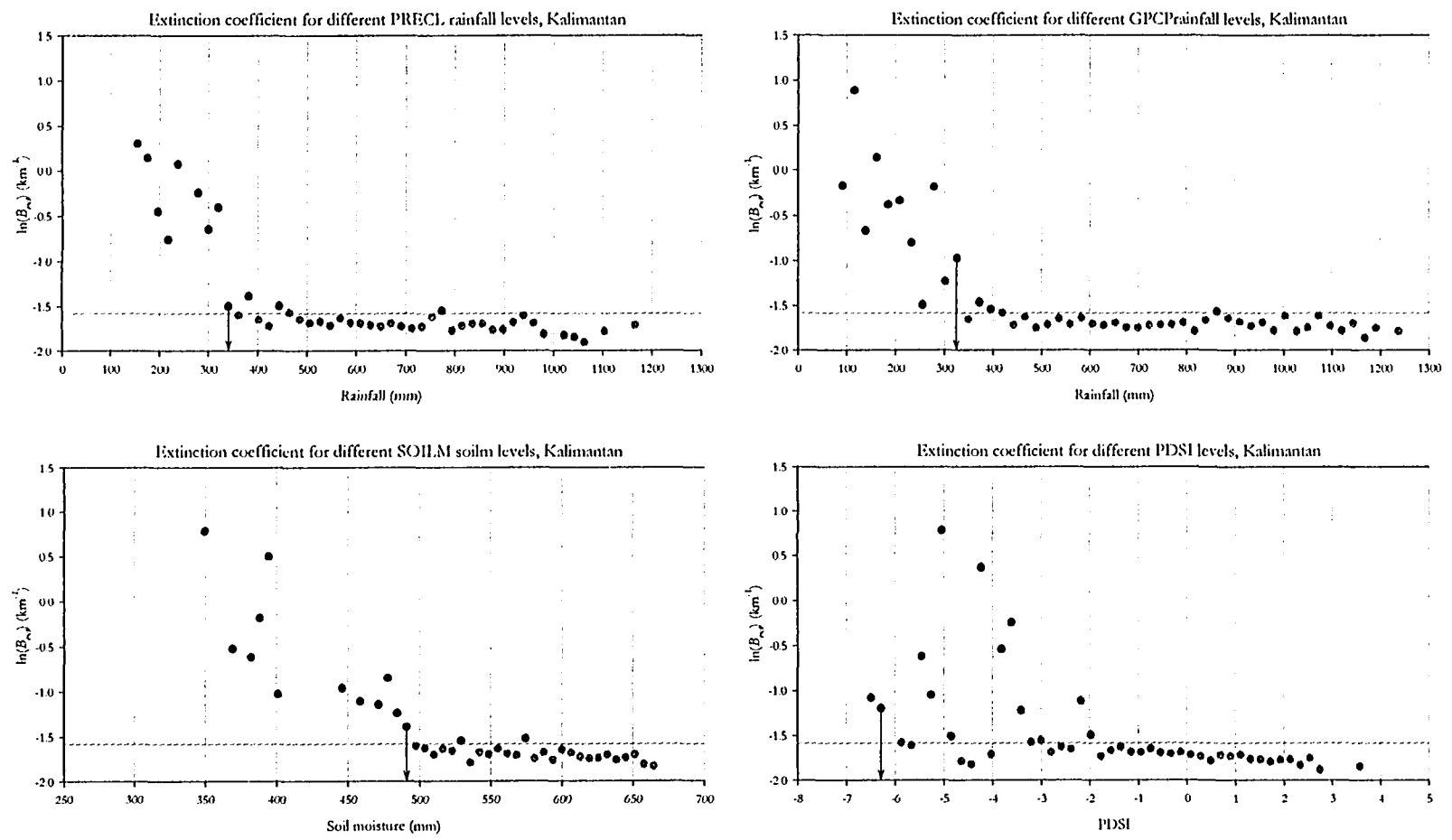


Figure 18. Interval-based thresholds for Kalimantan, PRECL (top left), GPCP (top right), SOILM (bottom left) and PDSI (bottom right). Black circles indicate class intervals significantly above the baseline value, grey circles indicate class intervals not significantly above the baseline, the grey horizontal line indicates the baseline value, and the black arrow indicates the threshold value.

	Sumatra				Kalimantan		
	Threshold	LCL	UCL		Threshold	LCL	UCL
PRECL				PRECL			
Change point	337.26	247.83	404.93	Change point	414.25	381.01	467.89
Sigmoidal	301.99	241.57	339.70	Sigmoidal	351.20	321.82	375.03
ALB	382.48			ALB	367.47		
Interval-based	346.44			Interval-based	340.61		
GPCP				GPCP			
Change point	273.97	211.89	316.73	Change point	378.65	272.40	455.81
Sigmoidal	237.71	192.69	263.19	Sigmoidal	294.71	225.95	341.29
ALB	204.58			ALB	298.77		
Interval-based	290.29			Interval-based	325.40		
SOILM				SOILM			
Change point	438.40	406.26	469.13	Change point	518.25	487.48	577.17
Sigmoidal	408.32	376.71	429.93	Sigmoidal	473.82	445.83	494.27
ALB	403.80			ALB	474.23		
Interval-based	419.37			Interval-based	490.92		
PDSI				PDSI			
Change point	-1.24	-2.39	-0.66	Change point	-1.53	-2.60	-1.01
Sigmoidal	-1.96	-4.40	8.40	Sigmoidal	-3.29	-4.50	-2.38
ALB	-1.97			ALB	-2.93		
Interval-based	-7.46			Interval-based	-6.28		

Table 4. Summary of moisture threshold estimates

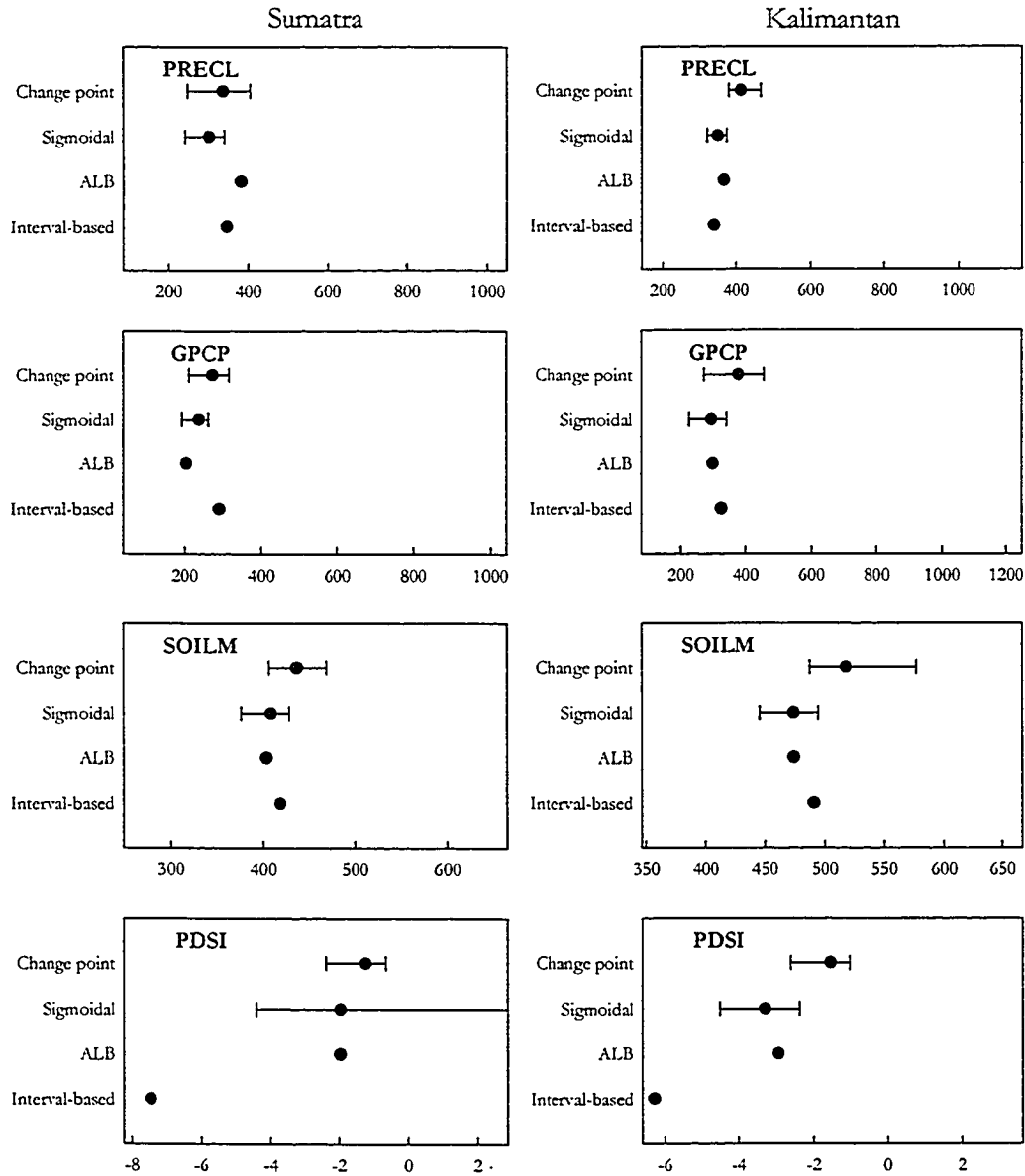


Figure 19. Threshold estimates for different moisture indices and models. Where applicable, error bars indicate 95% bootstrapped confidence intervals. Horizontal axes have been scaled according to the maximum and minimum values of each moisture index observed over each domain.

Operational guidelines

For operational use, it is preferable to use thresholds from a single moisture index, from among the candidate indices considered. From the regression results, the simple rainfall-derived indices from the PRECL and GPCP datasets performed better than the more complex SOILM and PDSI models. Between the PRECL and GPCP

datasets, neither emerged as a clearly superior product; the GPCP index was better in Sumatra, but the PRECL was better in Kalimantan. While individual products could be used for both analysis regions, it is preferable to choose a single product for consistency across regions. The PRECL index was therefore chosen because of its relative simplicity, although it must be emphasized that the GPCP index is also a worthy index, and that both indices are measuring the same region-wide rainfall.

Similar to Field et al. [2004], de Groot et al. [2005] and Dymond et al. [in press] simple interpretive guidelines for 3-month total rainfall, using the PRECL index are proposed for operational use. One possible set of guidelines is shown in Table 5, whose class delineations were derived as follows: The Extreme class boundary was set at the upper 95% confidence limit of the threshold, to err on the side of caution. The High class boundary was set at the 25th percentile of the 3-month total PRECL values and the Moderate class boundary at the 50th percentile of the 3-month total PRECL. For ease of interpretation, values were then rounded to the nearest 50mm to derive operational 3-month total rainfall classes. As suggested by Field et al. [2004] the classes below are derived for a broad area, and should be interpreted and adapted in the context of the local fire environment and management requirements. Furthermore, the guidelines are only applicable to the Indonesian region and should not be used in the drier, northern countries of Southeast Asia, or in other tropical regions.

	Sumatra		Kalimantan		Interpretation
	Class boundary	Suggested interval	Class boundary	Suggested interval	
Extreme	404.93	< 400mm	467.89	< 450mm	Extreme drought, severe haze probable
High	503.31	400mm - 500mm	574.63	450mm - 550mm	Approach normal dry-season peak conditions.
Moderate	680.31	500mm-700mm	746	550mm-750mm	Normal dry season conditions
Low		> 700mm		> 750mm	Normal wet season conditions

Table 5. 3-month rainfall interpretive guidelines for Sumatra and Kalimantan based on PRECL rainfall

5. Conclusions

5.1. Key results

A new proxy for smoke haze in Indonesia has been calculated, providing the best available record of smoke-haze to date for the whole country. Using synoptic weather observations archived at the NCDC, visibility data were available for two periods: from 1942 to 1965 and from 1973 to 2003, with the latter period showing a large improvement in data quality. Historical extinction coefficient signals were calculated for southern Sumatra and southern Kalimantan, by averaging across station observations. These signals were used to compare the relative magnitude of haze events from 1979 to 2002, a period of intense land-use change in Indonesia, but during which few quantitative comparisons exist. During the 1990's the sensitivity of the Indonesian fire environment appeared to increase due to increased land-use change, when judging by the haze response to underlying drought conditions, which is consistent with Nichol [1998], Siegert et al. [2001] and Hendon [2003]. The 1997 haze event was shown to be of an unprecedented magnitude, in terms of its atypically early onset, long duration and severity. The 1991 and 1994 events in Sumatra were also significant, and the 2002 event in Kalimantan was unexpectedly severe given the moderate drought conditions during that period. Should this pattern continue, a future drought on the order of the 1997 event, or even the 1991 or 1994 events, could result in unprecedented amount of haze.

Four different moisture indices were compared for their ability to predict haze events: the NCEP PRECL 3-month total rainfall, the NCEP GPCP 3-month total rainfall, the NCEP SOILM soil moisture model and the NCAR PDSI soil moisture model. Three nonlinear regression models were fit to the historical data with log-transformed extinction coefficient as the response, and each of the drought indices as predictor variable.

The PRECL and GPCP indices were shown to be the best overall predictors of haze. The SOILM model also performed reasonably well, but did not provide any advantage over the two simpler rainfall-derived indices and requires more extensive computation. The PDSI, as currently parameterized, was found to be inappropriate as

a drought monitoring tool for fire management in Indonesia, and should not be used operationally. This highlights the need to carefully consider the performance of drought monitoring tools developed for one region prior to application in another [Fogarty et al., 1998; Quiring and Papakryiakou, 2003]. Because of its satisfactory predictive performance in Sumatra and Kalimantan, and relative simplicity, the PRECL-based index is recommended as a seasonal drought indicator.

Of the nonlinear regression models considered, the ALB and change-point models had the most predictive power. The three-parameter sigmoid model was found to be under parameterized, and as a result did not fully capture the magnitude of haze events in Sumatra. The current method of estimating threshold values based on the gradient properties of the sigmoidal and ALB models was seen to yield lower threshold estimates than the change-point model. Closer examination of the gradient-based thresholds showed that these values could be too low to be useful as an early warning indicator of haze. The thresholds from the change point model were therefore adopted to form the basis of operational drought monitoring guidelines using the PRECL 3-month rainfall total. The threshold between normal and haze probable conditions was 337.26mm (247.83mm, 404.93mm) in Sumatra and 414.25mm (381.01mm, 467.89mm) in Kalimantan.

Interpretive classes were developed based on these threshold estimates to interpret seasonal rainfall conditions, which can be used to interpret current moisture conditions and medium-range rainfall forecasts. Operationally, 3-month running rainfall totals could be easily computed from real time data at national meteorological agencies for dissemination to forest management and emergency preparedness agencies, as a complement to the fire danger rating systems recently adopted by Indonesia [de Groot et al., in press]. Furthermore, these guidelines can be used to interpret seasonal rainfall forecasts currently being issued for the Indonesian region, for example the 3-month rainfall outlook of the European Centre for Medium Range Weather Forecasting.

5.2. Suggestions for further work

The work presented here could be extended in several directions. To improve the visibility dataset, efforts should be made to recover data from 1965 to 1973, during which no records were available for Indonesia. This period was the start of the official transmigration policies and increased population in the fire prone areas of Sumatra and Kalimantan [Fearnside, 1997], and included a strong El Niño event in 1972. Efforts should also be made to recover data from the early 1990's, which also saw a reduction in data quality, but appears as an important transition period in the sensitivity of the Indonesian fire environment to drought. Also, the heteroskedastic error variance found under all regression models could potentially be addressed using alternative bootstrap approaches, namely the 'wild bootstrap' approach described by Flachaire [2005].

Further improvements could be made to strengthen the use of the existing visibility observations, by further incorporating the qualitative present weather codes used for hydrometeor filtering. The present weather codes include a category for smoke haze, or specifically: "Visibility reduced by smoke, e.g. veldt or forest fires, industrial smoke or volcanic ashes" [NCDC, 2003]. These codes could be used to supplementary check on visibility observations. Godon and Toddhunter [1998], for example, successfully used the present weather codes to analyze dust storm occurrence in North Dakota, and attributed a decrease in dust storm frequency to improved farm management practices. Also, for broad distribution of the data set, it is typical to provide station data, and spatially gridded data, as illustrated by the distribution format of the NCEP and NCAR moisture datasets. Such a data-gridding exercise would ideally examine different the effectiveness of different interpolation algorithms for gridding visibility, as was done by Chen et al. [2002]'s gridding of precipitation.

Such improvements will strengthen future use of the haze dataset in developing early warning models. In this respect, an important avenue of investigation would be to broaden the range of causal factors of smoke haze beyond drought. Ultimately, Indonesian droughts coincide with warm phases of the ENSO cycle. Numerous

indices are available to quantify ENSO conditions; it would be useful from an early warning perspective to examine the relationship between historical ENSO conditions, drought and haze.

Also, this analysis has examined climatic factors exclusively as triggers of haze in Indonesia. For the sake of understanding the predisposing causes of the haze though, it will be important to understand the socio-economic and land management factors, perhaps as an extension of Stolle and Lambin's [2003] analysis of fire in Sumatra, to more rigorously understand the increase in sensitivity of the Indonesian fire environment to drought stress.

The new dataset is expected to support a wide range of other applications beyond the drought and haze analysis. Langmann and Heil [2004] modeled smoke emissions and transport from Indonesia, but only validated modeled concentrations against observations in Malaysia due to the lack of continuous air quality monitoring in Indonesia. With straightforward calibration as in, for example, O'Neill et al. [2002], visibility observations could be used as a particulate matter proxy, and used to validate modelled particulate concentration over a broader range of receptor distances. Long-term visibility observations calibrated as indicators of particulate matter could also be used to examine the long-term relationships between smoke haze exposure and human health, extending the shorter term studies of Frankenberg et al. [2005], for example.

Arguably, the largest scale impact of Indonesian smoke emissions is to the global climate system, when the magnitude of the emissions are compared to other sources, as was done by Page et al. [2002]. Outside of the 1997/98 event, no estimates of historical emissions from Indonesian biomass burning exist, representing a significant knowledge gap in global GHG emissions inventories. The visibility observations could form the basis for such an inventory, and then be used to determine the significance of the net radiative forcing due to Indonesian biomass burning using a simple energy-balance climate model. Such a study would determine whether Indonesian biomass burning emissions rank significantly among other major sources, such as fossil fuel emissions, in terms of their effect on the global climate. Should this

be the case, land-use reform in Indonesia will be a necessary addition to GHG emissions reduction strategies at a global scale, as has recently been suggested [Aldhous, 2004].

References

- Adler, R. F., G. J. Huffman, A. Chang, R. Ferraro, P. P. Xie, J. Janowiak, B. Rudolf, U. Schneider, S. Curtis, D. Bolvin, A. Gruber, J. Susskind, P. Arkin, and E. Nelkin, The Version-2 Global Precipitation Climatology Project (GPCP) Monthly Precipitation Analysis (1979-Present), *Journal of Hydrometeorology*, 4, 1147-1167, 2003.
- Aldhous, P., Land Remediation: Borneo Is Burning, *Nature*, 432, 144-146, 2004.
- American Meteorological Society, Meteorological Drought - Policy Statement, *Bulletin of the American Meteorological Society*, 78, 847-849, 1997.
- Applegate, G., Chokkalingam, U., and Suyanto. The Underlying Causes and Impacts of Fires in Southeast Asia: Final Report. 2001. Jakarta, Center for International Forestry Research.
- Asian Development Bank (ADB) and National Development Planning Agency (BAPPENAS). Causes, extent, impact and costs of 1997/98 fires and drought. Final report, Annex 1 and 2. Planning for Fire Prevention and Drought Management Project. 1999. Asian Development Bank TA 2999-INO Fortech. Pusat Pengembangan Agribisnis, Margueles Poyry, Jakarta, Indonesia.
- Bell, M. L., J. M. Samet, and F. Dominici, Time-Series Studies of Particulate Matter, *Annual Review of Public Health*, 25, 247-280, 2004.
- Bowen, M. R., J. M. Bompard, I. P. Anderson, P. Guizol, and A. Gouyon, Anthropogenic Fires in Indonesia: A View from Sumatra, in *Forest Fires and Regional Haze in Southeast Asia*, edited by P. Eaton, M. Radojevic, and (eds), pp. 41-66, Nova Science Publishers, Huntington, NY, 2001.
- Brasseur, G. P., J. T. Kiehl, J. F. Muller, T. Schneider, C. Granier, X. X. Tie, and D. Hauglustaine, Past and Future Changes in Global Tropospheric Ozone: Impact on Radiative Forcing, *Geophysical Research Letters*, 25, 3807-3810, 1998.
- Brauer, M. and S. Saksena, Accessible Tools for Classification of Exposure to Particles, *Chemosphere*, 49, 1151-1162, 2002.
- Burrows, J. P., M. Weber, M. Buchwitz, V. Rozanov, A. Ladstätter-Weissenmayer, A. Richter, R. Debeek, R. Hoogen, K. Bramstedt, K. U. Eichmann, and M. Eisinger, The Global Ozone Monitoring Experiment (GOME): Mission Concept and First Scientific Results, *Journal of the Atmospheric Sciences*, 56, 151-175, 1999.
- Chan, C. Y., L. Y. Chan, Y. G. Zheng, J. M. Harris, S. J. Oltmans, and S. Christopher, Effects of 1997 Indonesian Forest Fires on Tropospheric Ozone Enhancement, Radiative Forcing, and Temperature Change Over the Hong Kong Region, *Journal of Geophysical Research-Atmospheres*, 106, 14875-

14885, 2001.

Chandra, S., J. R. Ziemke, P. K. Bhartia, and R. V. Martin, Tropical Tropospheric Ozone: Implications for Dynamics and Biomass Burning, *Journal of Geophysical Research-Atmospheres*, 107, 2002.

Chandra, S., J. R. Ziemke, W. Min, and W. G. Read, Effects of 1997-1998 El Nino on Tropospheric Ozone and Water Vapor, *Geophysical Research Letters*, 25, 3867-3870, 1998.

Chen, M. Y., P. P. Xie, J. E. Janowiak, and P. A. Arkin, Global Land Precipitation: a 50-Yr Monthly Analysis Based on Gauge Observations, *Journal of Hydrometeorology*, 3, 249-266, 2002.

Cochrane, M. A., Fire Science for Rainforests, *Nature*, 421, 913-919, 2003.

Dai, A., K. E. Trenberth, and T. Qian, A Global Data Set of Palmer Drought Severity Index for 1870-2002: Relationship With Soil Moisture and Effects of Surface Warming, *Journal of Hydrometeorology*, 5, 1117-1130, 2004.

Davies, S. J. and Unam, L. Smoke-haze From the 1997 Indonesian Forest Fires: Effects on Pollution Levels, Local Climate, Atmospheric CO₂ Concentrations and Tree Photosynthesis. *Forest Ecology and Management*, 124, 137-144, 1999.

Davis, R. E., P. C. Knappenberger, P. J. Michaels, and W. M. Novicoff, Changing Heat-Related Mortality in the United States, *Environmental Health Perspectives*, 111, 1712-1718, 2003a.

Davis, R. E., P. C. Knappenberger, W. M. Novicoff, and P. J. Michaels, Decadal Changes in Summer Mortality in US Cities, *International Journal of Biometeorology*, 47, 166-175, 2003b.

de Groot, W. J., R. D. Field, M. A. Brady, O. Roswintiarti, and M. Mohamad, Development of the Indonesia and Malaysia Fire Danger Rating Systems, *Mitigation and Adaptation Strategies for Global Change*, in press.

de Groot, W. J., Wardati, and Y. H. Wang, Calibrating the Fine Fuel Moisture Code for Grass Ignition Potential in Sumatra, Indonesia, *International Journal of Wildland Fire*, 14, 161-168, 2005.

Delfino, R. J., M. R. Becklake, J. A. Hanley, and B. Singh, Estimation of Unmeasured Particulate Air-Pollution Data for an Epidemiologic-Study of Daily Respiratory Morbidity, *Environmental Research*, 67, 20-38, 1994.

Doyle, M. and S. Dorling, Visibility Trends in the UK 1950-1997, *Atmospheric Environment*, 36, 3161-3172, 2002.

- Duncan, B. N., R. V. Martin, A. C. Staudt, R. Yevich, and J. A. Logan, Interannual and Seasonal Variability of Biomass Burning Emissions Constrained by Satellite Observations, *Journal of Geophysical Research-Atmospheres*, 108, art. no.-4100, 2003.
- Efron, B. and Tibshirani, R. J. An Introduction to the Bootstrap. 436pp. 1993. Boca Raton, Chapman and Hall.
- Enhalt, D. and co-authors, Atmospheric Chemistry and Greenhouse Gases, in *Climate Change 2001: The Scientific Basis.*, edited by J.E. Houghton et al., pp. 239-287, Cambridge University Press, Cambridge, 2001.
- Fan, Y. and H. Van Den Dool, Climate Prediction Center Global Monthly Soil Moisture Data Set at 0.5 Degrees Resolution for 1948 to Present, *Journal of Geophysical Research-Atmospheres*, 109, 2004.
- Fang, M. and W. Huang, Tracking the Indonesian Forest Fire Using NOAA/AVHRR Images, *International Journal of Remote Sensing*, 19, 387-390, 1998.
- Fang, M., M. Zheng, F. Wang, K. L. To, A. B. Jaafar, and S. L. Tong, The Solvent-Extractable Organic Compounds in the Indonesia Biomass Burning Aerosols - Characterization Studies, *Atmospheric Environment*, 33, 783-795, 1999.
- Fearnside, P. M., Transmigration in Indonesia: Lessons From Its Environmental and Social Impacts, *Environmental Management*, 21, 553-570, 1997.
- Field, R. D., Y. Wang, O. Roswintiarti, and Guswanto, A Drought-Based Predictor of Recent Haze Events in Western Indonesia, *Atmospheric Environment*, 38, 1869-1878, 2004.
- Flachaire, E., Bootstrapping Heteroskedastic Regression Models: Wild Bootstrap Vs. Pairs Bootstrap, *Computational Statistics & Data Analysis*, 49, 361-376, 2005.
- Flannigan, M. D. and J. B. Harrington, A Study of the Relation of Meteorological Variables to Monthly Provincial Area Burned by Wildfire in Canada (1953-80), *Journal of Applied Meteorology*, 27, 441-452, 1988.
- Fogarty, L. G., Pearce, H. G., Catchpole, W. R., and Alexander, M. E. Adoption vs. Adaptation: Lessons From Applying the Canadian Forest Fire Danger Rating System in New Zealand. Viegas, D. X. Proceedings, Volume I: III International Conference on Forest Fire Research, 14th Conference on Fire and Forest Meteorology , 1011-1028, 1998.
- Frandsen, W. H., Ignition Probability of Organic Soils, *Canadian Journal of Forest Research-Revue Canadienne De Recherche Forestiere*, 27, 1471-1477, 1997.
- Frankenberg, E., D. Mckee, and D. Thomas, Health Consequences of Forest Fires in Indonesia, *Demography*, 42, 109-129, 2005.

- Fromm, M. D. and R. Servranckx, Transport of Forest Fire Smoke Above the Tropopause by Supercell Convection, *Geophysical Research Letters*, 30, Art. No. 1542, 2003.
- Fujiwara, M., K. Kita, S. Kawakami, T. Ogawa, N. Komala, S. Saraspriya, and A. Suropto, Tropospheric Ozone Enhancements During the Indonesian Forest Fire Events in 1994 and in 1997 as Revealed by Ground-Based Observations, *Geophysical Research Letters*, 26, 2417-2420, 1999.
- Gebremichael, M., W. F. Krajewski, M. Morrissey, D. Langerud, G. J. Huffman, and R. Adler, Error Uncertainty Analysis of GPCP Monthly Rainfall Products: a Data-Based Simulation Study, *Journal of Applied Meteorology*, 42, 1837-1848, 2003.
- Glover, D. and Jessup, T. Indonesia's Fires and Haze: The Cost of Catastrophe. 99. Singapore, Published jointly by the Institute of Southeast Asian Studies, Singapore and the International Development Research Centre, Ottawa, Canada. 1999.
- Godon, N. A. and P. E. Todhunter, A Climatology of Airborne Dust for the Red River Valley of North Dakota, *Atmospheric Environment*, 32, 1587-1594, 1998.
- Goldammer, J. G. and Seibert, B. The Impact of Droughts and Forest Fires on Tropical Lowland Rain Forest of East Kalimantan. Goldammer, J. G. Fire in the tropical biota: Ecosystem processes and global challenges. Proceedings of the Third Symposium on Fire Ecology, May 1989, Freiburg, Germany. Ecological Studies; Volume 84, 11-31. 1990. Heidelberg, Germany, Springer-Verlag. Billings, W. D., Golley, F., Lange, O. L., Olson, J. S., and Remmert, H.
- Gutman, G., I. Csiszar, and P. Romanov, Using NOAA/AVHRR Products to Monitor El Nino Impacts: Focus on Indonesia in 1997-98, *Bulletin of the American Meteorological Society*, 81, 1189-1205, 2000.
- Hartmann, D. L. Global Physical Climatology. 411. 1994. San Diego, CA, Academic Press.
- Hauglustaine, D. A., G. P. Brasseur, and J. S. Levine, A Sensitivity Simulation of Tropospheric Ozone Changes Due to the 1997 Indonesian Fire Emissions, *Geophysical Research Letters*, 26, 3305-3308, 1999.
- Heil, A. and J. G. Goldammer, Smoke-haze Pollution: A Review of the 1997 Episode in Southeast Asia, *Regional Environmental Change*, 24-37, 2001.
- Heim, R. R., A Review of Twentieth-Century Drought Indices Used in the United States, *Bulletin of the American Meteorological Society*, 83, 1149-1165, 2002.
- Hendon, H. H., Indonesian Rainfall Variability: Impacts of ENSO and Local Air-Sea

- Interaction, *Journal of Climate*, 16, 1775-1790, 2003.
- Herman, J. R., P. K. Bhartia, O. Torres, C. Hsu, C. Seftor, and E. Celarier, Global Distribution of UV-Absorbing Aerosols From Nimbus 7/TOMS Data, *Journal of Geophysical Research-Atmospheres*, 102, 16911-16922, 1997.
- Hessl, A. E. and L. J. Graumlich, Interactive Effects of Human Activities, Herbivory and Fire on Quaking Aspen (*Populus Tremuloides*) Age Structures in Western Wyoming, *Journal of Biogeography*, 29, 889-902, 2002.
- Hessl, A. E., D. Mckenzie, and R. Schellhaas, Drought and Pacific Decadal Oscillation Linked to Fire Occurrence in the Inland Pacific Northwest, *Ecological Applications*, 14, 425-442, 2004.
- Hooper, P. M., Flexible Regression Modeling With Adaptive Logistic Basis Functions, *Canadian Journal of Statistics-Revue Canadienne De Statistique*, 29, 343-364, 2001.
- Hsu, N. C., J. R. Herman, P. K. Bhartia, C. J. Seftor, O. Torres, A. M. Thompson, J. F. Gleason, T. F. Eck, and B. N. Holben, Detection of Biomass Burning Smoke From TOMS Measurements, *Geophysical Research Letters*, 23, 745-748, 1996.
- Hsu, N. C., J. R. Herman, O. Torres, B. N. Holben, D. Tanre, T. F. Eck, A. Smirnov, B. Chatenet, and F. Lavenu, Comparisons of the TOMS Aerosol Index With Sun-Photometer Aerosol Optical Thickness: Results and Applications, *Journal of Geophysical Research-Atmospheres*, 104, 6269-6279, 1999.
- Husar, R. B., J. M. Holloway, D. E. Patterson, and W. E. Wilson, Spatial and Temporal Pattern of Eastern-United-States Haziness - a Summary, *Atmospheric Environment*, 15, 1919-1928, 1981.
- Husar, R. B., J. D. Husar, and L. Martin, Distribution of Continental Surface Aerosol Extinction Based on Visual Range Data, *Atmospheric Environment*, 34, 5067-5078, 2000.
- Ikegami, M., K. Okada, Y. Zaizen, Y. Makino, J. B. Jensen, J. L. Gras, and H. Harjanto, Very High Weight Ratios of S/K in Individual Haze Particles Over Kalimantan During the 1997 Indonesian Forest Fires, *Atmospheric Environment*, 35, 4237-4243, 2001.
- Jacobson, M. Z., *Atmospheric Pollution: History, Science and Regulation*, Cambridge University Press, Cambridge, UK., 2002.
- Kaiser, D. P. and Y. Qian, Decreasing Trends in Sunshine Duration Over China for 1954-1998: Indication of Increased Haze Pollution?, *Geophysical Research Letters*, 29, 2002.

- Kalnay, E., M. Kanamitsu, R. Kistler, W. Collins, D. Deaven, L. Gandin, M. Iredell, S. Saha, G. White, J. Woollen, Y. Zhu, M. Chelliah, W. Ebisuzaki, W. Higgins, J. Janowiak, K. C. Mo, C. Ropelewski, J. Wang, A. Leetmaa, R. Reynolds, R. Jenne, and D. Joseph, The NCEP/NCAR 40-Year Reanalysis Project, *Bulletin of the American Meteorological Society*, 77, 437-471, 1996.
- Khandekar, M. L., T. S. Murty, D. Scott, and W. Baird, The 1997 El Nino, Indonesian Forest Fires and the Malaysian Smoke Problem: a Deadly Combination of Natural and Man-Made Hazard, *Natural Hazards*, 21, 131-144, 2000.
- Kita, K., M. Fujiwara, and S. Kawakami, Total ozone increase associated with forest fires over the Indonesian region and its relation to the El Niño-Southern oscillation, *Atmospheric Environment*, 34, 2681-2690, 2000.
- Knorr, W., M. Scholze, N. Gobron, B. Pinty, and T. Kaminski, Global Scale Drought Caused Atmospheric CO₂ Increase, *EOS Transactions*, 86, 178, 181, 2005.
- Kunii, O., S. Kanagawa, I. Yajima, Y. Hisamatsu, S. Yamamura, T. Amagai, and I. T. S. Ismail, The 1997 Haze Disaster in Indonesia: Its Air Quality and Health Effects, *Archives of Environmental Health*, 57, 16-22, 2002.
- Langenfelds, R. L., R. J. Francey, B. C. Pak, L. P. Steele, J. Lloyd, C. M. Trudinger, and C. E. Allison, Interannual Growth Rate Variations of Atmospheric CO₂ and Its Delta C-13, H-2, CH₄, and CO Between 1992 and 1999 Linked to Biomass Burning, *Global Biogeochemical Cycles*, 16, 2002.
- Langmann, B. and A. Heil, Release and Dispersion of Vegetation and Peat Fire Emissions in the Atmosphere Over Indonesia 1997/1998, *Atmospheric Chemistry and Physics*, 4, 2145-2160, 2004.
- Levine, J. S., The 1997 Fires in Kalimantan and Sumatra, Indonesia: Gaseous and Particulate Emissions, *Geophysical Research Letters*, 26, 815-818, 1999.
- Liew, S. C., L. K. Kwok, K. Padmanabhan, O. K. Lim, and H. Lim, Delineating Land/Forest Fire Burnt Scars With ERS Interferometric Synthetic Aperture Radar, *Geophysical Research Letters*, 26, 2409-2412, 1999.
- McDonnell, W. F., N. Nishino-Ishikawa, F. F. Petersen, L. H. Chen, and D. E. Abbey, Relationships of Mortality With the Fine and Coarse Fractions of Long-Term Ambient PM₁₀ Concentrations in Nonsmokers, *Journal of Exposure Analysis and Environmental Epidemiology*, 10, 427-436, 2000.
- Menz, K., K. Ellis, C. Conroy, and P. Grist, Fire as an Economic Disincentive to Smallholder Rubber Planting in Imperata Areas of Indonesia, *Environmental Modelling & Software*, 14, 27-35, 1999.
- Nakajima, T., A. Higurashi, N. Takeuchi, and J. R. Herman, Satellite and Ground-

Based Study of Optical Properties of 1997 Indonesian Forest Fire Aerosols, *Geophysical Research Letters*, 26, 2421-2424, 1999.

- Nasi, R., E. Dennis, E. Meijaard, G. Applegate, and P. Moore, Forest Fire and Biological Diversity, *Unasylva*, 53, 36-40, 2002.
- National Climatic Data Center (NCDC). Data documentation for data set 3505 (DSI-3505) Integrated Surface Hourly Data. 2003. Asheville, NC., National Oceanic and Atmospheric Administration, National Climatic Data Center.
- Neter, J., Kutner, M. H., Nachtsheim, C. J., and Wasserman, W. Applied Linear Statistical models. 1996. Boston, MA, McGraw-Hill.
- Nichol, J., Smoke Haze in Southeast Asia: a Predictable Recurrence, *Atmospheric Environment*, 32, 2715-2716, 1998.
- Nichol, J., Bioclimatic impacts of the 1994 smoke haze event in Southeast Asia, *Atmospheric Environment*, 31, 1209-1219, 1997.
- Nicholls, N., The Insignificance of Significance Testing, *Bulletin of the American Meteorological Society*, 82, 981-986, 2001.
- Ntale, H. K. and T. Y. Gan, Drought Indices and Their Application to East Africa, *International Journal of Climatology*, 23, 1335-1357, 2003.
- O'Neill, M. S., D. Loomis, V. T. Meza, A. Retama, and D. Gold, Estimating Particle Exposure in the Mexico City Metropolitan Area, *Journal of Exposure Analysis and Environmental Epidemiology*, 12, 145-156, 2002.
- Olson, D. M., E. Dinerstein, E. D. Wikramanayake, N. D. Burgess, G. V. N. Powell, E. C. Underwood, J. A. D'amico, I. Itoua, H. E. Strand, J. C. Morrison, C. J. Loucks, T. F. Allnutt, T. H. Ricketts, Y. Kura, J. F. Lamoreux, W. W. Wettengel, P. Hedao, and K. R. Kassem, Terrestrial Ecoregions of the Worlds: a New Map of Life on Earth, *Bioscience*, 51, 933-938, 2001.
- Page, C. M., N. Nicholls, N. Plummer, B. Trewin, M. Manton, L. Alexander, L. E. Chambers, Y. Choi, D. A. Collins, A. Gosai, P. Della-Marta, M. R. Haylock, K. Inape, V. Laurent, L. Maitrepierre, E. E. P. Makmur, H. Nakamigawa, N. Ouprasitwong, S. McGree, J. Pahailad, M. J. Salinger, L. Tibig, T. D. Tran, K. Vediapan, and P. Zhai, Data Rescue in the Southeast Asia and South Pacific Region - Challenges and Opportunities, *Bulletin of the American Meteorological Society*, 85, 1483-1489, 2004.
- Page, S. E., F. Siegert, J. O. Rieley, H. D. V. Boehm, A. Jaya, and S. Limin, The Amount of Carbon Released From Peat and Forest Fires in Indonesia During 1997, *Nature*, 420, 61-65, 2002.
- Palmer, W. C. Meteorological Drought. 1965. Washington, DC., United States

Weather Bureau.

- Podgorny, I. A., F. Li, and V. Ramanathan, Large Aerosol Radiative Forcing Due to the 1997 Indonesian Forest Fire, *Geophysical Research Letters*, 30, art. no.-1028, 2003.
- Qian, Y. and F. Giorgi, Regional Climatic Effects of Anthropogenic Aerosols? The Case of Southwestern China, *Geophysical Research Letters*, 27, 3521-3524, 2000.
- Quiring, S. M. and T. N. Papakryiakou, An Evaluation of Agricultural Drought Indices for the Canadian Prairies, *Agricultural and Forest Meteorology*, 118, 49-62, 2003.
- Radojevic, M., Chemistry of Forest Fires and Regional Haze With Emphasis on Southeast Asia, *Pure and Applied Geophysics*, 160, 157-187, 2003.
- Sastry, N., Forest Fires, Air Pollution, and Mortality in Southeast Asia, *Demography*, 39, 1-23, 2002.
- Sawa, Y., H. Matsueda, Y. Tsutsumi, J. B. Jensen, H. Y. Inoue, and Y. Makino, Tropospheric Carbon Monoxide and Hydrogen Measurements Over Kalimantan in Indonesia and Northern Australia During October, 1997, *Geophysical Research Letters*, 26, 1389-1392, 1999.
- Schichtel, B. A., R. B. Husar, S. R. Falke, and W. E. Wilson, Haze Trends Over the United States, 1980-1995, *Atmospheric Environment*, 35, 5205-5210, 2001.
- Seber, G. A. F. and Wild, C. J. Nonlinear Regression. 1989. New York, John Wiley and Sons.
- Siegert, F., G. Ruecker, A. Hinrichs, and A. A. Hoffmann, Increased Damage From Fires in Logged Forests During Droughts Caused by El Nino, *Nature*, 414, 437-440, 2001.
- Siegert, F. and A. A. Hoffmann, The 1998 forest fires in East Kalimantan (Indonesia): a quantitative evaluation using high resolution, multitemporal ERS-2 SAR images and NOAA-AVHRR hotspot data, *Remote Sensing of Environment*, 72, 64-77, 2000.
- Stolle, F. and E. F. Lambin, Interprovincial and Interannual Differences in the Causes of Land-Use Fires in Sumatra, Indonesia, *Environmental Conservation*, 30, 375-387, 2003.
- Sudo, K. and M. Takahashi, Simulation of Tropospheric Ozone Changes During 1997-1998 El Nino: Meteorological Impact on Tropospheric Photochemistry, *Geophysical Research Letters*, 28, 4091-4094, 2001.

- Thompson, A. M., J. C. Witte, R. D. Hudson, H. Guo, J. R. Herman, and M. Fujiwara, Tropical Tropospheric Ozone and Biomass Burning, *Science*, 291, 2128-2132, 2001.
- Tomich, T. P., Fagi, A. M., de Foresta, H., Michon, G., Murdiyarso, D., Stolle, F., and van Noordwijk, M. Indonesia's Fires: Smoke as a Problem, Smoke as a Symptom. *Agroforestry Today* 10(1), 4-7. 1998. London, UK, International Centre for Research in Agroforestry (ICRAF).
- Toms, J. D. and M. L. Lesperance, Piecewise Regression: a Tool for Identifying Ecological Thresholds, *Ecology*, 84, 2034-2041, 2003.
- Tsai, Y. I., Y. H. Lin, and S. Z. Lee, Visibility Variation With Air Qualities in the Metropolitan Area in Southern Taiwan, *Water Air and Soil Pollution*, 144, 19-40, 2003.
- Tsutsumi, Y., Y. Sawa, Y. Makino, J. B. Jensen, J. L. Gras, B. F. Ryan, S. Diharjo, and H. Harjanto, Aircraft Measurements of Ozone, Nox, Co, and Aerosol Concentrations in Biomass Burning Smoke Over Indonesia and Australia in October 1997: Depleted Ozone Layer at Low Altitude Over Indonesia, *Geophysical Research Letters*, 26, 595-598, 1999.
- Van Der Werf, G. R., J. T. Randerson, G. J. Collatz, L. Giglio, P. S. Kasibhatla, A. F. Arellano, S. C. Olsen, and E. S. Kasischke, Continental-Scale Partitioning of Fire Emissions During the 1997 to 2001 El Nino/La Nina Period, *Science*, 303, 73-76, 2004.
- Van Nieuwstadt, M. G. L. and D. Sheil, Drought, Fire and Tree Survival in a Borneo Rain Forest, East Kalimantan, Indonesia, *Journal of Ecology*, 93, 191-201, 2005.
- Von Hoyningen-Huene, W., T. Schmidt, S. Schienbein, C. A. Kee, and L. J. Tick, Climate-Relevant Aerosol Parameters of South-East-Asian Forest Fire Haze, *Atmospheric Environment*, 33, 3183-3190, 1999.
- Wang, Y. H., R. D. Field, and O. Roswintiarti, Trends in Atmospheric Haze Induced by Peat Fires in Sumatra Island, Indonesia and El Nino Phenomenon From 1973 to 2003, *Geophysical Research Letters*, 31, 2004.
- Westerling, A. L., A. Gershunov, D. R. Cayan, and T. P. Barnett, Long Lead Statistical Forecasts of Area Burned in Western US Wildfires by Ecosystem Province, *International Journal of Wildland Fire*, 11, 257-266, 2002.
- World Meteorological Organization, Guide to Meteorological Instruments and Methods of Observation, World Meteorological Organization, Geneva, Switzerland, 1996.
- World Meteorological Organization. International Meteorological Vocabulary. 1992.

World Meteorological Organization.

Wotton, B. M., D. L. Martell, and K. A. Logan, Climate Change and People-Caused Forest Fire Occurrence in Ontario, *Climatic Change*, 60, 275-295, 2003.

Yadav, A. K., K. Kumar, A. Kasim, M. P. Singh, S. K. Parida, and M. Sharan, Visibility and Incidence of Respiratory Diseases During the 1998 Haze Episode in Brunei Darussalam, *Pure and Applied Geophysics*, 160, 265-277, 2003.

Yoneda, T., S. Nishimura, and Chairul, Impacts of Dry and Hazy Weather in 1997 on a Tropical Rainforest Ecosystem in West Sumatra, Indonesia, *Ecological Research*, 15, 63-71, 2000.

Yonemura, S., H. Tsuruta, S. Kawashima, S. Sudo, L. C. Peng, L. S. Fook, Z. Johar, and M. Hayashi, Tropospheric Ozone Climatology Over Peninsular Malaysia From 1992 to 1999, *Journal of Geophysical Research-Atmospheres*, 107, art. no.-4229, 2002a.

Yonemura, S., H. Tsuruta, T. Maeda, S. Kawashima, S. Sudo, and M. Hayashi, Tropospheric Ozone Variability Over Singapore From August 1996 to December 1999, *Atmospheric Environment*, 36, 2061-2070, 2002b.

Zeng, N., A. Mariotti, and P. Wetzel, Terrestrial Mechanisms of Interannual CO₂ Variability, *Global Biogeochemical Cycles*, 19, 2005.

Ziemke, J. R. and S. Chandra, La Nina and El Nino-Induced Variabilities of Ozone in the Tropical Lower Atmosphere During 1970-2001, *Geophysical Research Letters*, 30, art. no.-1142, 2003.

Appendix A: Model parameter estimates and residuals

		Sumatra				
		MEAN	S.E.	LCL	UCL	Fits
PRECL	β_0	1.2851	0.6354	0.2448	2.2214	968
	β_1	-0.0087	0.0050	-0.0143	-0.0046	
	β_2	0.0086	0.0049	0.0045	0.0141	
	α	337.26	42.45	247.83	404.93	
GPCP	β_0	1.1412	0.4824	0.2338	2.1917	958
	β_1	-0.0099	0.0027	-0.0168	-0.0058	
	β_2	0.0098	0.0027	0.0057	0.0166	
	α	273.97	26.25	211.89	316.73	
SOILM	β_0	4.1934	1.1573	2.2659	6.5259	963
	β_1	-0.0131	0.0030	-0.0196	-0.0082	
	β_2	0.0127	0.0029	0.0080	0.0190	
	α	438.40	16.76	406.26	469.13	
PDSI	β_0	-1.8429	0.2867	-2.5410	-1.6266	663
	β_1	-0.2040	0.0984	-0.4431	-0.0979	
	β_2	0.1984	0.0978	0.0846	0.4309	
	α	-1.24	0.47	-2.39	-0.66	
		Kalimantan				
		MEAN	S.E.	LCL	UCL	Fits
PRECL	β_0	1.1209	0.5446	0.1305	2.2472	833
	β_1	-0.0067	0.0015	-0.0099	-0.0038	
	β_2	0.0067	0.0015	0.0039	0.0099	
	α	414.25	22.37	381.01	467.89	
GPCP	β_0	0.4703	0.6474	-0.4514	1.7481	881
	β_1	-0.0058	0.0032	-0.0120	-0.0027	
	β_2	0.0058	0.0032	0.0027	0.0119	
	α	378.65	43.75	272.40	455.81	
SOILM	β_0	3.1650	1.2683	0.8617	5.6369	816
	β_1	-0.0093	0.0029	-0.0144	-0.0044	
	β_2	0.0090	0.0028	0.0048	0.0140	
	α	518.25	20.71	487.48	577.17	
PDSI	β_0	-1.9215	0.1622	-2.3680	-1.7399	553
	β_1	-0.1925	0.0605	-0.3488	-0.1042	
	β_2	0.1861	0.0591	0.0946	0.3306	
	α	-1.53	0.40	-2.60	-1.01	

Table 6. Bootstrapped parameter estimates for change point models, including the mean, standard error, 95% marginal confidence intervals and total number of successful fits.

		Sumatra				
		MEAN	S.E.	LCL	UCL	Fits
PRECL	A	-1.57	0.01	-1.58	-1.55	999
	B	46.33	13.15	17.41	72.20	
	x_0	240.98	22.99	194.51	282.08	
	Threshold	301.99	25.06	241.57	339.70	
GPCP	A	-1.56	0.01	-1.58	-1.55	993
	B	35.41	11.07	16.18	59.41	
	x_0	191.07	16.83	148.38	217.58	
	Threshold	237.71	18.35	192.69	263.19	
SOILM	A	-1.57	0.01	-1.59	-1.55	991
	B	22.01	9.71	2.25	40.67	
	x_0	379.33	10.29	354.69	398.65	
	Threshold	408.32	14.03	376.71	429.93	
PDSI	A	-1.79	1.05	-2.61	-1.54	973
	B	2.51	3.17	0.09	10.93	
	x_0	-4.71	4.08	-8.79	-3.16	
	Threshold	-1.96	3.63	-4.40	8.40	
		Kalimantan				
		MEAN	S.E.	LCL	UCL	Fits
PRECL	A	-1.62	0.01	-1.64	-1.60	1000
	B	45.80	18.43	14.69	82.86	
	x_0	290.88	26.49	230.38	328.11	
	Threshold	351.20	14.18	321.82	375.03	
GPCP	A	-1.62	0.01	-1.64	-1.60	989
	B	63.07	22.99	19.43	111.64	
	x_0	211.65	33.43	129.71	264.31	
	Threshold	294.71	30.33	225.95	341.29	
SOILM	A	-1.65	0.02	-1.69	-1.61	993
	B	38.09	11.29	16.10	62.97	
	x_0	423.65	18.41	384.95	458.50	
	Threshold	473.82	14.05	445.83	494.27	
PDSI	A	-1.72	0.05	-1.83	-1.61	999
	B	1.96	0.84	0.12	3.67	
	x_0	-5.87	1.31	-8.60	-3.56	
	Threshold	-3.29	0.59	-4.50	-2.38	

Table 7. Bootstrapped parameter estimates for sigmoidal models, including the mean, standard error, 95% marginal confidence intervals and total number of successful fits.

Sumatra					Kalimantan						
	K	tau	dlta	gma	rpt		K	tau	dlta	gma	rpt
PRECL	5	0.758				PRECL	2	1.757			
	1		-0.230	0.034	1.219		1		3.999	-0.234	-6.088
	2		8.853	-0.097	-3.870		2		-0.212	0.234	2.305
	3		-0.215	0.152	0.105						
	4		2.256	-1.005	-1.607						
	5		-0.309	0.916	-0.632						
GPCP	2	1.658				GPCP	2	1.754			
	1		-0.211	0.309	0.835		1		-0.205	0.284	1.286
	2		6.514	-0.309	-5.048		2		4.781	-0.284	-5.214
SOILM	2	1.686				SOILM	2	1.900			
	1		-0.244	0.198	-0.691		1		-0.295	-0.034	-1.419
	2		6.107	-0.198	-4.054		2		4.952	0.034	-4.077
PDSI	10	0.561				PDSI	2	1.486			
	1		-0.134	0.400	-0.401		1		-0.195	0.207	2.386
	2		-0.077	0.013	1.018		2		2.140	-0.207	-5.090
	3		-0.445	0.379	-0.602						
	4		1.787	0.250	-1.364						
	5		9.394	-2.308	-2.677						
	6		0.554	0.245	-1.522						
	7		0.410	0.950	-4.342						
	8		-0.232	0.065	0.241						
	9		-0.285	0.034	0.717						
	10		-0.408	-0.027	1.570						

Table 8. Parameter estimates for ALB model

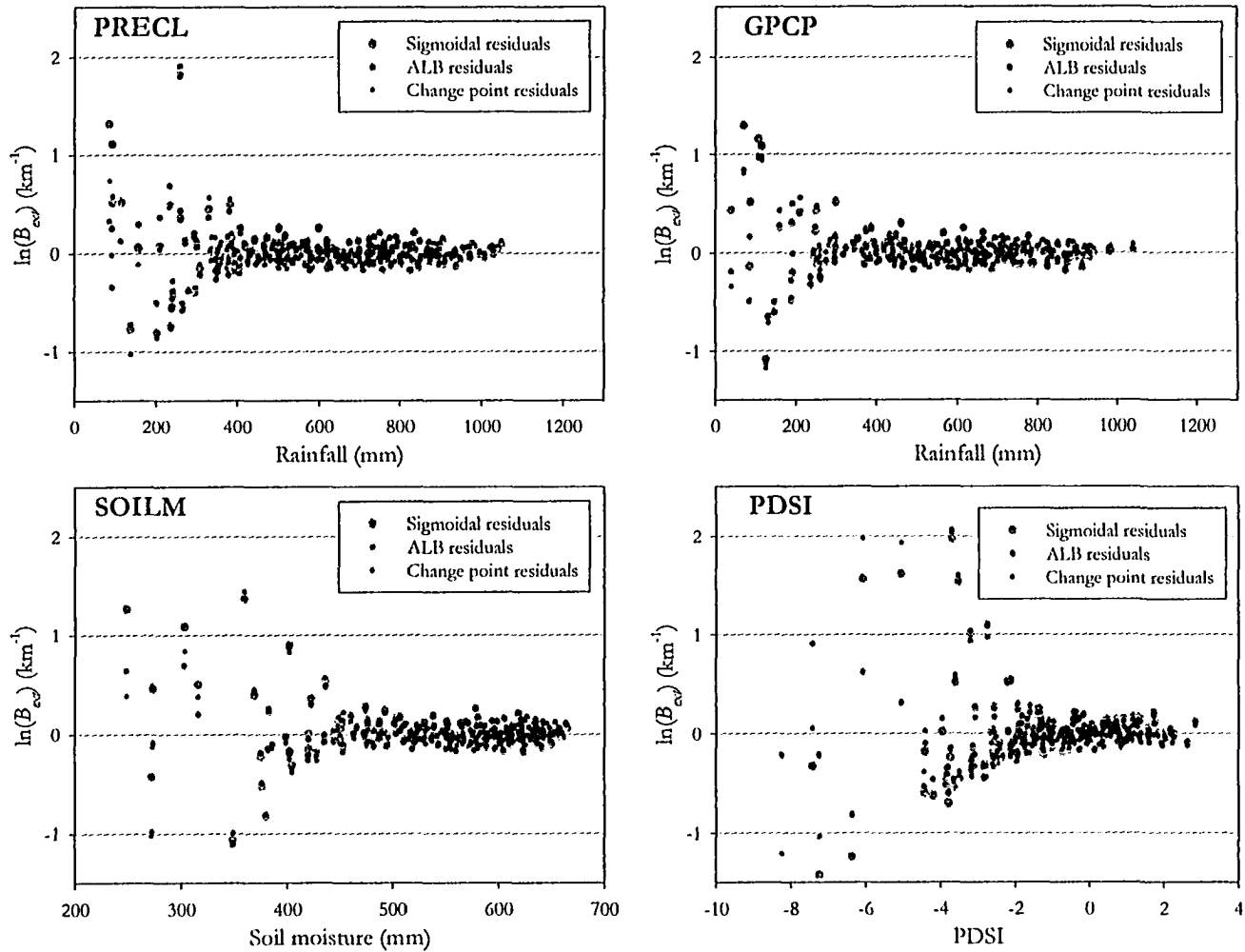


Figure 20. Residuals from fitted models for Sumatra.

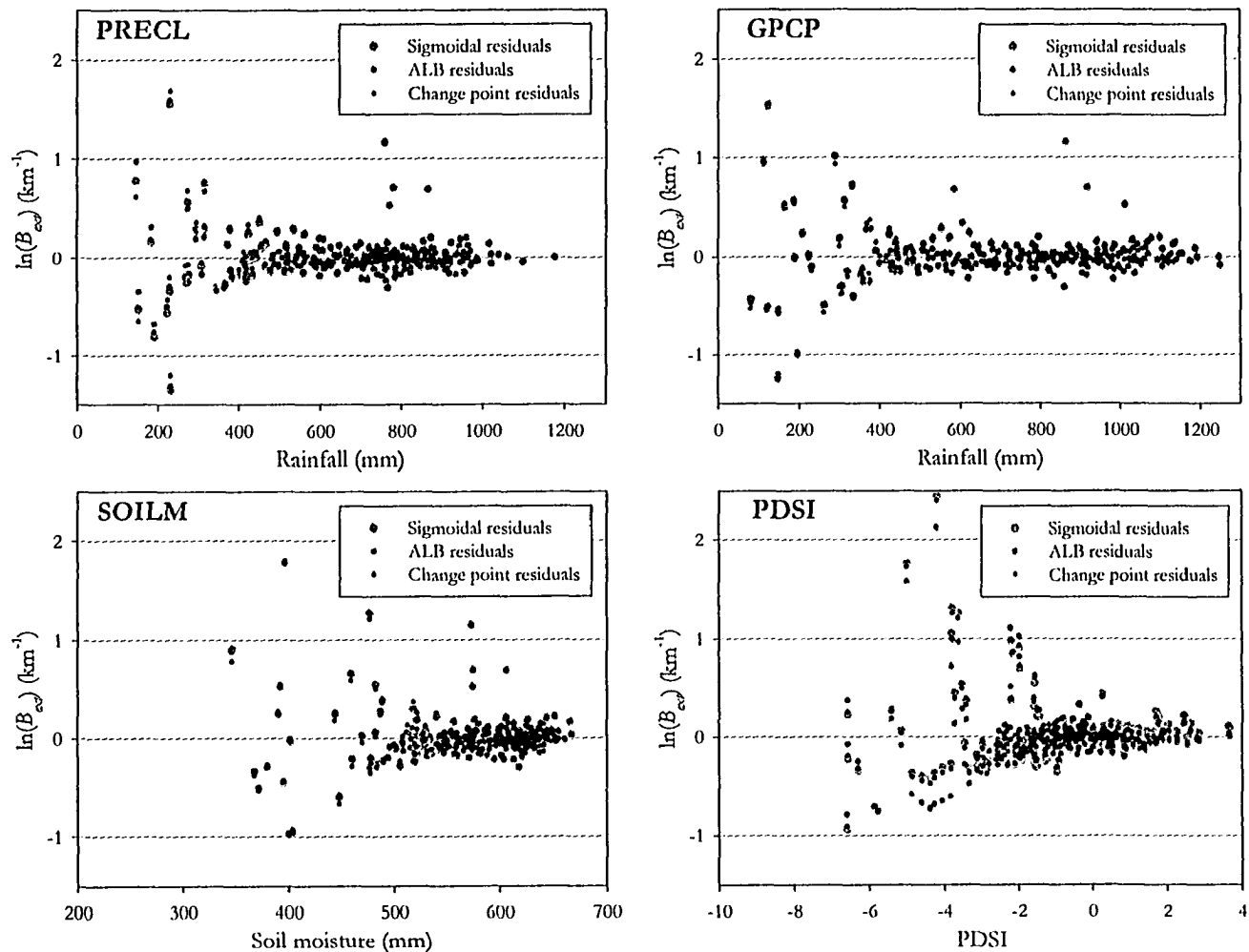


Figure 21. Residuals from fitted models for Kalimantan.